Acetonitrile and cyanide compounds containing metal–metal bonds: syntheses, structures and applications to solid-state chemistry

Stuart L. Bartley, Stacey N. Bernstein and Kim R. Dunbar*

Department of Chemistry and the Center for Fundamental Materials Research, Michigan State University, East Lansing, MI 48824 (USA)

(Received April 22, 1993)

Abstract

Compounds with acetonitrile and cyanide ligands have been prepared from mild substitution reactions of well-known metal–metal bonded precursors. Facile non-redox substitution of the carboxylate ligands in $Mo_2(O_2CCH_3)_4$ occurs in chlorinated solvents treated with excess $[R_4N][CN]$ (R = Et, Bu^n) to produce the salts $[R_4N]_4[Mo_2(CN)_8]$ (R = Et (**3**); Bu^n (**1**)) in high yields. These reactions were found to be solvent dependent, with the major product isolated from reactions performed in THF being $[Bu^n{}_4N]_3[Mo_2(O_2CCH_3)(CN)_6]$ (**2**). The chloride ligands in multiply-bonded dirhenium compounds are readily displaced by cyanide as demonstrated by the reaction between $Re_2Cl_4(dppm)_2$ and $[Bu^n{}_4N]CN$ to give $[Bu^n{}_4N]_2[Re_2(CN)_6(dppm)_2]$ (**4**). Compounds **1–4** were characterized by IR and electronic spectroscopies; single crystal X-ray data were collected for **1**, **2** and **4**. **1**·8$CHCl_3$: orthorhombic, *Pbca*, $a = 20.526(8)$, $b = 28.122(5)$, $c = 19.855(7)$ Å, $V = 11461(4)$ Å^3, $R = 0.082$, $R_w = 0.083$; **2**: monoclinic, $P2_1$, $a = 12.046(3)$, $b = 16.050(10)$, $c = 16.854(3)$ Å, $\beta = 94.11(2)°$, $V = 3250(2)$ Å^3, $R = 0.067$, $R_w = 0.067$; **4**·8CH_2Cl_2: triclinic, $P\bar{1}$, $a = 13.835(2)$, $b = 18.172(2)$, $c = 12.261(1)$ Å, $\alpha = 106.788(8)$, $\beta = 107.850(9)$, $\gamma = 93.894(9)°$, $V = 2767.5(6)$ Å^3, $R = 0.041$, $R_w = 0.045$. The molecular structure of $[Bu^n{}_4N]_4[Mo_2(CN)_8]$ contains dimolybdenum(II) centers ligated by eight CN^- ligands in the familiar unbridged M_2L_8 arrangement, with the two $Mo(CN)_4$ units being perfectly eclipsed as expected for a molecule with a δ component to the M–M bond. The Mo–Mo distance of 2.122(2) Å is the shortest reported distance for an unbridged homoleptic $Mo_2^{II,II}L_8$ compound. The related salt, $[Bu^n{}_4N]_3[Mo_2(O_2CCH_3)(CN_6]$ (**2**), contains an anion displaying a structure similar to **1**, but with one bridging acetate ligand, the presence of which results in a slight contraction of the Mo–Mo bond to 2.114(2) Å. The hexacyanodirhenium compound, **4**, is reminiscent of M(III) complexes of the type $M_2X_6(dppm)_2$ with one important exception, namely it is of the type $[M_2X_6(dppm)_2]^{2-}$ with divalent metal centers. The equatorial plane in **4**, bisected by two *trans* dppm ligands, consists of four unidentate terminal cyanide ligands and two cyanide groups that adopt an unusual η^2-(σ,π) bridging arrangement. The Re–Re distance of 3.0505(6) Å is formally a single bond based on the conventional overlap scheme for a d^5–d^5 M_2L_{10} compound, viz. $\sigma^2\pi^2(\delta^2\delta^{*2})\pi^{*2}$; this assignment is supported by the diamagnetism of the compound as revealed by NMR and magnetic susceptibility studies. With the exception of the bridging cyanides in **4**, the ν(CN) stretches in the new compounds **1–4** occur at higher frequencies than free CN^-, indicating that they are acting purely as donors. In related chemistry, the alkylcyanide CH_3CN is used as the sole supporting ligand in dinuclear metal cations. The compounds $[Bu^n{}_4N]_2[Re_2Cl_8]$ and $Re_2Cl_4(PPr^n{}_3)_4$ react with HBF_4 etherate solutions to yield the hitherto unknown compound $[Re_2(MeCN)_{10}][BF_4]_4$ (**5**), containing a triply-bonded solvated cation. Compound **5** and the previously reported salts $[M_2(MeCN)_{10}][BF_4]_4$ (M = Mo, Rh) were metathesized with $[Bu^n{}_4N]_2[M_6O_{19}]$ (M = Mo, W) and $[Bu^n{}_4N]_4[Mo_8O_{26}]$ in MeCN to give $[M_2(MeCN)_{10}][M'_6O_{19}]_2$ (M = Re, M' = Mo (**6**); M = Rh, M' = Mo (**7**); M = Rh, M' = W (**9**); M = M' = Mo (**10**); M = Mo, M' = W (**12**)) and $[M_2(MeCN)_{10}][M'_8O_{26}]$ (M = Rh (**8**); M' = Mo (**11**)). The products were isolated directly from acetonitrile solutions as insoluble salts and characterized primarily by IR and UV–Vis spectroscopies which are diagnostic tools for the presence of the M–M bonded chromophore with coordinated nitrile ligands as well as the intact polyoxometallate anions. Layering of the two separate salt solutions led to the isolation of single crystals in two cases. Crystal data for representative salts are: **6**·4CH_3CN·2H_2O: monoclinic *C*2/*c*, $a = 18.36(2)$, $b = 22.67(2)$, $c = 17.45(2)$ Å, $\beta = 90.31(9)°$, $V = 7263(13)$ Å^3, $R = 0.066$, $R_w = 0.083$; **7**·4CH_3CN: monoclinic *C*2/*c*, $a = 18.457(2)$, $b = 22.723(2)$, $c = 17.190(2)$ Å, $\beta = 90.07(1)°$, $V = 7209(2)$ Å^3, $R = 0.079$, $R_w = 0.059$. Compounds **6** and **7** were subjected to thermal gravimetric analysis and found to undergo quantitative loss of acetonitrile solvent ligands to give amorphous metal oxide materials of empirical composition MMo_6O_{19} (M = Rh (**13**); Re (**15**)). The anaerobic thermal treatment of $[Mo_2(MeCN)_{10}][Mo_6O_{19}]_2$ (**10**) leads to a crystalline material of empirical formula $Mo'Mo_6O_{19}$ (**14**) whose powder X-ray pattern revealed tetragonal symmetry with unit cell dimensions $a = b = 10.811(1)$, $c = 2.819(8)$ Å, $V = 329.56(6)$ Å^3. These results will be discussed along with the cyanide chemistry in light of the design of new ordered materials starting from metal–metal bonded molecules.

*Author to whom correspondence should be addressed.

0020-1693/93/$6.00

Introduction

During the last three decades [1a], dinuclear complexes with metal–metal bonds have graduated from the realm of chemical curiosities to a richly developed class of compounds with well-understood structural and electronic properties [1b]. A variety of σ and π donors are known to stabilize these compounds, the most common being phosphine, halide and carboxylate ligands. While these ligand types have been cornerstones in the development of metal–metal bonding in the molecular regime, with a few exceptions, they have not been particularly amenable to the design of extended structures from multiply-bonded precursors [2]. Two underexplored classes of compounds that hold promise for expanding the chemistry of metal–metal bonded molecules to solids are nitrile and cyanide complexes. General synthetic strategies to these compounds, key spectroscopic properties and single crystal X-ray structures are presented along with applications of dinuclear acetonitrile cations to the low temperature syntheses of new metal oxides. Some of these results have been reported in preliminary communications [3, 4].

Experimental

Starting materials

The compounds $Mo_2(O_2CCH_3)_4$ [5], $Mo_2(O_2CCF_3)_4$ [6], $[Rh_2(MeCN)_{10}](BF_4)_4$ [7], $[Mo_2(MeCN)_{10}](BF_4)_4$ [8], $Re_2Cl_4(dppm)_4$ [9], $[Bu^n{}_4N]_2[Re_2Cl_8]$ [10] and $Re_2Cl_4(PPr^n{}_3)_4$ [11] were prepared according to literature methods. The polyoxometallate salts $[Bu^n{}_4N]_2[Mo_6O_{19}]$ [12], $[Bu^n{}_4N]_2[W_6O_{19}]$ [13], $[Bu^n{}_4N]_4[Mo_8O_{26}]$ [13] and the soluble cyanide salt $[Et_4N]CN$ [14] were prepared by standard procedures. The reagents $[Bu^n{}_4N]CN$ and $HBF_4 \cdot Et_2O$ were purchased from Aldrich Chemicals and used without further purification. Tetrahydrofuran, toluene, and hexanes were freshly distilled from sodium/potassium benzophenone ketyl. Dichloromethane and chloroform were distilled from P_2O_5 and acetonitrile was distilled from CaH_2. Dimethylacetamide (DMAA) and nitromethane were purchased from Aldrich and purged with dinitrogen before use.

Reaction procedures

All operations were carried out under an atmosphere of dry nitrogen or argon by using standard Schlenk-line techniques. For the cyanide chemistry, all glassware was flame dried under vacuum prior to use.

Preparation of cyanide compounds

$[Bu^n{}_4N]_4[Mo_2(CN)_8]$ (1)

A $CHCl_3$ (8 ml) solution containing $[Bu^n{}_4N]CN$ (0.534 g, 1.99 mmol) was added to $Mo_2(O_2CCH_3)_4$ (0.106 g, 0.248 mmol) dissolved in 4 ml of $CHCl_3$ to give a dark purple reaction solution which was stirred at r.t. for 5 days during which time the color changed to blue. Addition of hexanes (5 ml) followed by cooling to 0 °C for 2 days led to the precipitation of a bright blue crystalline solid. After a second addition of hexanes (2 ml) and chilling at 0 °C for 1 day, the product was collected by filtration, washed with hexanes (3×3 ml) and dried *in vacuo*. Yield 0.133 g (40%). *Anal.* Calc. for $C_{72}H_{144}N_{12}Mo_2$: C, 63.13; H, 10.60; N, 12.27. Found: C, 61.63; H, 10.75; N, 11.54%. The low values for the carbon and nitrogen analyses are attributed to residual $CHCl_3$ trapped in the crystalline form of the sample; this is supported by X-ray data that reveal the presence of 8 $CHCl_3$ molecules per $[Mo_2(CN)_8]^{4-}$ anion in the crystal form. IR (CsI plates, Nujol mull, cm^{-1}): 2095s, 1153m, 1107w, 1060w, 1030w, 968w, 887m, 801w.

$[Bu^n{}_4N]_3[Mo_2(O_2CCH_3)(CN)_6]$ (2)

In a typical reaction, a solution consisting of $[Bu^n{}_4N]CN$ (1.427 g, 5.31 mmol) in 10 ml of THF was slowly added to a sample of $Mo_2(O_2CCH_3)_4$ (0.379 g, 0.88 mmol) in 10 ml of THF to give a dark purple solution. The reaction was stirred at r.t. for 5 min during which time a red–purple solid precipitated. Additional product was harvested in the form of red–purple microcrystals that appeared after the reaction mixture was left undisturbed for 12 h; the crystals were collected by filtration, washed with THF (2×10 ml) and dried *in vacuo*. Yield 0.93 g (92%). *Anal.* Calc. for $C_{56}H_{111}N_9O_2Mo_2$: C, 59.29; H, 9.86; N, 11.11. Found: C, 59.05; H, 9.63; N, 10.78%. IR (CsI plates, Nujol mull, cm^{-1}): 2105m, 2099m, 1604w, 1531w, 1154m, 1026w, 887m, 673m. UV–Vis (CH_2Cl_2): λ_{max} (nm) (ϵ (M^{-1} cm^{-1})) 557 (2.5×10^3), 276 (5.4×10^3).

$[Et_4N]_4[Mo_2(CN)_8]$ (3)

Method (i). To a flask charged with $Mo_2(O_2CCH_3)_4$ (0.100 g, 0.234 mmol) and $[Et_4N]CN$ (0.488 g, 3.12 mmol) was added 10 ml of CH_2Cl_2 which resulted in the formation of a blue solution. The reaction mixture was stirred at r.t. for 3 h, during which time a bright blue precipitate formed, which was collected by filtration, washed with CH_2Cl_2 (3×5 ml) and dried *in vacuo*. Yield 0.172 g (80%). IR (CsI plates, Nujol mull, cm^{-1}): 2095s, 1490m, 1323w, 1176s, 1003m, 788m, 666w, 390w, 358w, 293w. UV–Vis (CH_2Cl_2): λ_{max} (nm) (ϵ (M^{-1} cm^{-1})) 601 (3.0×10^3), 277 (4.9×10^3).

Method (ii). A flask containing $[Bu^n{}_4N]_3[Mo_2(O_2CCH_3)(CN)_6]$ (0.100 g, 0.088 mmol), $[Bu_4N]CN$ (0.095 g, 0.35 mmol) and 10 ml of CH_2Cl_2 was treated with $[Et_4N]Cl$ (0.146 g, 0.88 mmol) in 5 ml of CH_2Cl_2. A reaction swiftly ensued with the deposition of a bright blue precipitate. The reaction mixture was stirred for 12 h at r.t. after which time the solid was collected

by filtration and washed with CH_2Cl_2 (3×5 ml). Yield 0.071 g (88%).

$[Bu^n_4N]_2[Re_2(CN)_6(dppm)_2]$ (4)

The salt $[Bu^n_4N]CN$ (0.133 g, 0.50 mmol) in 5 ml of CH_2Cl_2 was added to a solution of $Re_2Cl_4(dppm)_2$ (0.100 g, 0.078 mmol) in 10 ml of CH_2Cl_2, leading to the formation of a green solution with concomitant deposition of a green microcrystalline solid within 5 min. The solution was reduced in volume to 5 ml and the product was collected by filtration, washed with toluene (3×5 ml) and dried *in vacuo*. Yield 0.093 g (67%). IR (CsI plates, Nujol mull, cm^{-1}): 2097w, 2081m, 1935w, 1900m, 1871w, 1589vw, 1308w, 1150m, 1094m, 1030m, 970w, 891m, 775m, 737m, 689m, 519m, 490m. The compound is virtually insoluble in all common solvents including THF and alcohols, and is only sparingly soluble in CH_3CN and CH_2Cl_2. The product was recrystallized from CH_2Cl_2 as the dichloromethane solvate $[Bu^n_4N]_2[Re_2(CN)_6(dppm)_2]\cdot 8CH_2Cl_2$. ^1H NMR (CD_3CN, 22 °C, 300 MHz): δ 7.48 (mult, 16H, Ph); 6.96 (mult, 24H, Ph); 5.44 (s, 16H, CH_2Cl_2); 3.30 (pentet, 4H, $-CH_2-$); Bu^n_4N: 3.05 (mult, 16H); 1.58 (mult, 16H); 1.33 (sextet, 16H), 0.95 (triplet, 24H). $^{31}P\{^1H\}$ NMR (CD_3CN, 22 °C relative to 85% H_3PO_4): −11.39 ppm. UV–Vis (CH_3CN): λ_{max} (nm) (ϵ (M^{-1} cm^{-1})) 969 (2.5×10^2), 694 (1.4×10^2).

Preparation of a new triply-bonded dinuclear acetonitrile cation

$[Re_2(MeCN)_{8-10}][BF_4]_4$ (5)

Method (i). A sample of $[Bu^n_4N]_2[Re_2Cl_8]$ (1.00 g, 0.865 mmol) was dissolved in 50 ml of CH_3CN and treated with 5 ml of $HBF_4\cdot Et_2O$ (85% HBF_4 solution). Following addition of the acid, the reaction was subjected to several evacuation and purge cycles to remove gaseous HCl after which time CH_2Cl_2 (200 ml) was slowly introduced into the reaction solution. The reaction was refluxed for 5 h, and the intensely colored blue solid that formed was collected, washed with CH_2Cl_2 and Et_2O and dried *in vacuo*. Yield 0.150 g (15%). IR (KBr plates, Nujol mull, cm^{-1}): ν(C≡N) = 2328m, 2295w; ν(B–F) = 1025vs, 520s. Partial loss of axial CH_3CN ligands leads to elemental analyses that vary for independent samples. A ^1H NMR spectrum in CD_3NO_2 of a sample subjected to a prolonged dynamic vacuum exhibits a resonance at $\delta = +3.39$ ppm and a minor feature at $\delta = +2.00$ ppm attributed to equatorial and axial CH_3CN groups, respectively. Similarly, in CD_3CN the ^1H NMR spectrum displays a shifted resonance at $\delta = +3.37$ ppm and a signal at +1.95 ppm where free CH_3CN occurs. UV–Vis (CH_3CN): λ_{max} (nm) (ϵ, (M^{-1} cm^{-1})) 866sh, 663 (6.3×10^2), 593 (5.9×10^2), 458sh, 244 (2.7×10^4), 203 (5.1×10^4). $E_{1/2}$ (red) = +0.24 V, $E_{p,c(1)} = -0.20$, $E_{p,c(2)} = -0.76$ V versus Ag/AgCl at a Pt bead electrode.

Method (ii). A quantity of $Re_2Cl_4(PPr^n_3)_4$ (0.350 g, 0.303 mmol) was suspended in a mixture of CH_3CN (10 ml) and CH_2Cl_2 (3 ml) and treated with 1 ml of $HBF_4\cdot Et_2O$ with periodic pumping and filling. The reaction solution turned green within 5 min and gradually became blue. After refluxing for 12 h, the solution was treated with 20 ml of CH_2Cl_2 to yield a bright blue solid which was collected by filtration, washed with CH_2Cl_2 and Et_2O, and dried *in vacuo*. Yield 0.253 g (80%).

Incorporation of the cations $[M_2(MeCN)_{10}]^{4+}$ (M = Mo, Re, Rh) into polyoxometallate salts

$[Re_2(MeCN)_{10}][Mo_6O_{19}]_2$ (6)

A quantity of $[Re_2(MeCN)_{10}][BF_4]_4$ (0.0335 g, 0.032 mmol) dissolved in CH_3CN (5 ml) was added dropwise to a vigorously stirring CH_3CN (5 ml) solution of $[Bu^n_4N]_2[Mo_6O_{19}]$ (0.055 g, 0.022 mmol) to form a blue–green microcrystalline solid. The solid was washed with two 10 ml portions of CH_3CN and dried *in vacuo* whereupon the solid turned blue–gray; yield 0.055 g of dry material (69%). Elemental analyses of typical samples prepared in this manner are low in carbon and nitrogen due to the loss of varying amounts of the axial CH_3CN ligands, a common occurrence for salts of $[M_2(MeCN)_{10}]^{4+}$ cations [8]. The following analysis best fits the formula $[Re_2(MeCN)_{8.5}][Mo_6O_{19}]_2$. *Anal.* Calc. for $Re_2Mo_{12}O_{38}N_{8.5}C_{17}H_{25.5}$: N, 4.80; C, 8.23; H, 1.04. Found: N, 4.78; C, 8.39; H, 1.20%. IR (KBr plates, Nujol mull, cm^{-1}): ν(C≡N) = 2350m, 2285w, 2250w; ν(Mo–O) = 956vs (br), 793vs (br), 598m (br), 492m (br). UV–Vis (DMAA): λ_{max} (nm) 715, 552, 324.

$[Rh_2(MeCN)_{10}][Mo_6O_{19}]_2$ (7)

A quantity of $[Rh_2(MeCN)_{10}][BF_4]_4$ (0.034 g, 0.035 mmol) was dissolved in 5 ml of CH_3CN and added to a stirring solution of $[Bu^n_4N]_2[Mo_6O_{19}]$ (0.096 g, 0.070 mmol) in 5 ml of CH_3CN. The precipitate that formed was isolated by decanting the colorless supernatant via cannula, washed with fresh CH_3CN and finally vacuum dried. Yield 0.071 g (86%) of microcrystalline orange solid. *Anal.* Calc. for $Rh_2Mo_{12}O_{38}N_{10}C_{20}H_{30}$: C, 10.11; H, 1.27; N, 5.90. Found: C, 10.30; H, 1.27; N, 5.16%. IR (KBr plates, Nujol mull, cm^{-1}): ν(C≡N) = 2336ms, 2310ms, 2282w; ν(Mo–O) = 963vs (br), 800vs (br), 597ms (br), 429m (br). UV–Vis (DMAA): λ_{max} (nm) 519, 318.

$[Rh_2(MeCN)_{10}][Mo_8O_{26}]$ (8)

A solution of $[Bu^n_4N]_4[Mo_8O_{26}]$ (0.082 g, 0.056 mmol) in 10 ml of CH_3CN was added via syringe to a stirring solution of $[Rh_2(MeCN)_{10}][BF_4]_4$ (0.054 g, 0.056 mmol) in 10 ml of CH_3CN to form a finely divided, pale orange solid. After stirring for 5 min, the solid was isolated from the colorless filtrate, washed with fresh CH_3CN and Et_2O, and dried under a stream of argon for 2 h

to yield 0.071 g of product (71%). IR (KBr plates, Nujol mull, cm^{-1}): ν(C≡N) = 2336ms, 2311ms, 2247w; ν(Mo–O) = 948vs, 913s, 845ms, 806m, 714s (br), 556w (sh), 522w. UV–Vis (DMAA): λ_{max} (nm) 519.

$[Rh_2(MeCN)_{10}][W_6O_{19}]_2$ (9)

Samples of $[Rh_2(MeCN)_{10}][BF_4]_4$ (0.025 g, 0.025 mmol) and $[Bu^n_4N]_2[W_6O_{19}]$ (0.095 g, 0.050 mmol) were dissolved in CH_3CN (10 ml) and stirred for 5 min. The resulting product was separated from the clear supernatant, washed with fresh CH_3CN and vacuum dried to yield 0.075 g (88%) of microcrystalline orange solid. IR (KBr plates, Nujol mull, cm^{-1}): ν(C≡N) = 2337s, 2310s, 2283w, 2249vw, 2242vw; ν(W–O) = 982vs (br), 814vs (br), 585ms, 444ms (br). UV–Vis (DMAA): λ_{max} (nm) 519.

$[Mo_2(MeCN)_8][Mo_6O_{19}]_2$ (10)

A solution of $[Mo_2(MeCN)_{10}][BF_4]_4$ (0.025 g, 0.053 mmol) in 5 ml of CH_3CN was added via syringe to a stirring solution of $[Bu^n_4N]_2[Mo_6O_{19}]$ (0.144 g, 0.106 mmol) in 5 ml of CH_3CN. The resulting blue precipitate was washed with fresh CH_3CN, and dried *in vacuo* to yield 0.115 g of a blue–green product (92%). IR (KBr plates, Nujol mull, cm^{-1}): ν(C≡N) = 2315m, 2284ms, 2255w; ν(Mo–O) = 972vs (br), 800vs (br), 600ms (br), 416ms (br). UV–Vis (DMAA): λ_{max} (nm) 718, 324.

$[Mo_2(MeCN)_8][Mo_8O_{26}]$ (11)

A 10 ml CH_3CN solution of $[Bu^n_4N]_4[Mo_8O_{26}]$ (0.068 g, 0.046 mmol) was slowly added to a stirring solution of $[Mo_2(MeCN)_{10}][BF_4]_4$ (0.040 g, 0.046 mmol) in 10 ml of CH_3CN to yield a black solid. After stirring for 10 min, the solid was removed by filtration, washed with copious amounts of CH_3CN and 10 ml of Et_2O and dried *in vacuo*. Yield 0.058 g (74%) of product. IR (KBr plates, Nujol mull, cm^{-1}): ν(C≡N) = 2321w, 2315vw, 2257w; ν(Mo–O) = 980s, 717vs (br), 486m.

$[Mo_2(MeCN)_8][W_6O_{19}]_2$ (12)

To a flask containing $[Mo_2(MeCN)_{10}][BF_4]_4$ (0.044 g, 0.046 mmol) and $[Bu^n_4N]_2[W_6O_{19}]$ (0.174 g, 0.092 mmol) was added 10 ml of CH_3CN. The reaction mixture was stirred vigorously for 5 min and then filtered to isolate a bright blue solid. The solid was washed with CH_3CN and dried under a dynamic vacuum to yield 0.140 g of product (89%). IR (KBr plates, Nujol mull, cm^{-1}): ν(C≡N) = 2316m, 2284s, 2255w; ν(W–O) = 991vs (br), 810vs (br), 586s, 443s (br).

Desolvation of polyoxometallate salts to form new oxide materials

Desolvation of the three $[Mo_6O_{19}]^{2-}$ containing salts, viz. **6**, **7** and **10**, was followed by thermogravimetric analysis under a dinitrogen atmosphere. The temperature at which complete loss of CH_3CN was achieved was ~350 °C at a rate of 1 °C/min. When the rate is increased, however, the final temperature required for complete desolvation was considerably less than 350 °C. These data reveal that loss of the coordinated acetonitrile ligands is essentially quantitative. The new oxide materials of empirical formula $M'Mo_6O_{19}$ (M' = Rh (**13**); Mo (**14**); Re (**15**)) are insoluble black solids; the desolvation product of $[Mo_2(MeCN)_8][Mo_6O_{19}]_2$ (**14**) is a highly pure crystalline phase as evidenced by powder X-ray diffraction.

Physical measurements

IR spectra were recorded on a Perkin-Elmer 599 or a Nicolet 740 FT-IR spectrometer. ^1H NMR spectra were measured on a Varian 300-MHz spectrometer. Chemical shifts were referenced relative to the residual proton impurities of methylene-d_2-chloride (5.32 ppm with respect to TMS), acetonitrile-d_3 (1.93 ppm with respect to TMS), or chloroform-d (7.24 ppm with respect to TMS). Elemental analyses were performed at Desert Analytics. Thermal gravimetric experiments were performed on a Cahn TGA 121. Samples were placed inside a quartz bucket and heated at 1 °C/min under a dinitrogen atmosphere. The temperature method included isotherms at 30 (20 min), 250 (60 min), 300 (60 min), 320 (30 min) and 350 (30 min) °C. Bulk samples were prepared by using a Lindberg single-zone tube furnace model 5934 equipped with an Omega CN-2012 programmable temperature controller. Samples of ~2.0 g were loaded into a quartz tube and purged with N_2 during heating which was carried out at a rate of 1°/min from 30 to 350 °C.

Single crystal X-ray crystallography

Structures were determined by application of general procedures fully described elsewhere [15]. Crystallographic data for $[Bu^n_4N]_4[Mo_2(CN)_8]\cdot 8CHCl_3$ (**1**·$8CHCl_3$), $[Bu^n_4N]_3[Mo_2(O_2CCH_3)CN)_8]$ (**2**), $[Bu^n_4N]_2[Re_2(CN)_6(dppm)_2]\cdot 8CH_2Cl_2$ (**4**·$8CH_2Cl_2$) and $[Re_2(MeCN)_{10}][Mo_6O_{19}]_2$ (**6**·$4CH_3CN\cdot 2H_2O$) were collected on a Rigaku AFC6S diffractometer with monochromated Mo Kα ($\lambda\bar{\alpha}$ = 0.71069 Å) radiation. Data for $[Rh_2(MeCN)_{10}][Mo_6O_{19}]_2$ (**7**·$4CH_3CN$) were obtained on a Nicolet P3/F upgraded to a Siemens P3/V diffractometer with Cu Kα radiation ($\lambda\bar{\alpha}$ = 1.5418 Å). All data were corrected for Lorentz and polarization effects. Calculations were performed on a VAXSTATION 2000 computer by using the Texsan crystallographic software package of the Molecular Structure Corporation [16]. Crystallographic data for the five compounds are compiled in Table 1 and positional parameters are listed in Tables 2–6.

TABLE 1. Crystal data for $[Bu^n_4N]_4[Mo_2(CN)_8]\cdot 8CHCl_3$ (**1**·8CHCl$_3$), $[Bu^n_4N]_3[Mo_2(OAc)CN)_8]$ (**2**), $[Bu^n_4N]_2Re_2(CN)_6(dppm)_2]\cdot 8CH_2Cl_2$ (**4**·8CH$_2$Cl$_2$), $[Re_2(MeCN)_{10}][Mo_6O_{19}]$ (**6**·4CH$_3$CN·2H$_2$O) and $[Rh_2(MeCN)_{10}][Mo_6O_{19}]$ (**7**·4CH$_3$CN)

	1·8CHCl$_3$	**2**	**4**·8CH$_2$Cl$_2$	**6**·4CH$_3$CN·2H$_2$O	**7**·4CH$_3$CN
Formula	$Mo_2C_{80}N_{12}Cl_{24}H_{152}$	$Mo_2C_{56}N_9O_2H_{111}$	$Re_2Cl_{16}P_4C_{96}N_8H_{132}$	$Re_2N_{14}C_{28}Mo_{12}O_{40}H_{46}$	$Rh_2N_{14}C_{36}Mo_{12}O_{38}H_{42}$
Formula weight	2324.92	1134.43	2461.70	2742.44	2636.03
Space group	*Pbca* (No. 61)	$P2_1$ (No. 4)	$P\bar{1}$ (No. 2)	*C*2/*c* (No. 15)	*C*2/*c* (No. 15)
a (Å)	20.526 (8)	12.046 (3)	13.835 (2)	18.36 (2)	18.457 (2)
b (Å)	28.122 (5)	16.05 (1)	18.172 (2)	22.67 (2)	22.723 (2)
c (Å)	19.855 (7)	16.854 (3)	12.261 (1)	17.45 (2)	17.190 (2)
α (°)	90	90	106.788 (8)	90	90
β (°)	90	94.11 (2)	107.850 (9)	90.31 (9)	90.07 (1)
γ (°)	90	90	93.894 (9)	90	90
V (Å^3)	11461 (4)	3250 (2)	2767.5 (6)	7263 (13)	7209 (2)
Z	4	2	1	4	4
D_{calc} (g/cm^3)	1.347	1.159	1.477	2.508	2.301
μ (Mo Kα) (cm^{-1})	8.20	4.16	27.06	54.03	213.470
Radiation (monochromated in incident beam)	Mo Kα ($\lambda\bar{\alpha}$=0.71069 Å)		Mo Kα ($\lambda\bar{\alpha}$=0.71069 Å)		Cu Kα ($\lambda\bar{\alpha}$=1.54184 Å)
Temperature (°C)	−100	−100	−100	−90	−75
Transmission factors: max., min.	1.00, 0.68	1.00, 0.24	1.00, 0.64	1.00, 0.46	1.00, 0.39
R[a]	0.082	0.067	0.041	0.066	0.079
R_w[b]	0.083	0.067	0.045	0.083	0.059

[a] $R=\Sigma\|\|F_o\|-|F_c\|\|/\Sigma|F_o|$. [b] $R_w=[\Sigma_w(|F_o|-|F_c|)^2/\Sigma w|F_o|^2]^{1/2}$; $w=1/\sigma^2(|F_o|)$.

$[Bu^n_4N]_4[Mo_2(CN)_8]\cdot 8CHCl_3$ (1·8CHCl$_3$)

Suitable crystals of $[Bu_4N]_4[Mo_2(CN)_8]\cdot 8CHCl_3$ were grown by slow diffusion of hexanes into a $CHCl_3$ solution of the compound in a flame sealed 8 mm O.D. glass tube at 25 °C. A blue crystal of dimensions $0.40\times0.50\times0.40$ mm was mounted on a glass fiber. Cell constants and an orientation matrix for data collection obtained from a least-squares refinement using the setting angles of 25 carefully centered reflections in the range $15\leqslant 2\theta\leqslant 24°$ corresponded to an orthorhombic cell. A total of 10 963 data was collected at -100 ± 1 °C using the ω-scan technique to a maximum 2θ value of 50°. The intensities of three representative reflections measured after every 150 reflections decreased by 6.1% thus a linear correction factor was applied to the data to account for this decay. A correction for secondary extinction was applied (coefficient = 0.19919E-07).

The systematic absences in the data led to the space group *Pbca*. The structure was solved by MITHRIL [17] and DIRDIF [18] structure programs and refined by full matrix least-squares refinement. After isotropic convergence had been achieved, an empirical absorption correction was applied using the program DIFABS [19], which resulted in transmission factors ranging from 0.68 to 1.00. All non-hydrogen atoms were refined with anisotropic thermal parameters whereas hydrogen atoms were placed in calculated positions for the final stages of refinement. The final cycle of full matrix least-squares refinement included 4972 observed reflections with $F_o^2>3\sigma(F_o^2)$ and 533 variable parameters to give $R=0.082$ and $R_w=0.083$ and a quality-of-fit index of 4.03.

$[Bu_4N]_3[Mo_2(O_2CCH_3)(CN)_6]$ (2)

Large red–purple crystals of $[Bu_4N]_3[Mo_2(O_2CCH_3)(CN)_6]$ were grown by slow diffusion of Et_2O into a CH_2Cl_2 solution of the compound in a flame sealed 8 mm O.D. glass tube at room temperature. A crystal of dimensions $0.72\times0.23\times0.47$ mm was mounted on the tip of a glass fiber and secured with silicone grease. Cell constants and an orientation matrix for data collection, obtained from a least-squares refinement using the setting angles of 16 carefully centered reflections in the range $20\leqslant 2\theta\leqslant 27°$, corresponded to a monoclinic cell. A total of 6240 reflections was measured at -100 ± 1 °C to a maximum 2θ value of 50° using the ω–2θ scan technique. The crystal diffracted poorly due to a large mosaic spread and only 3108 unique reflections were of the intensity $F_o^2>3\sigma(F_o^2)$. Three check reflections measured every 200 data points declined by 1.3% which was accounted for by a linear correction factor. A correction for secondary extinction was also applied (coefficient = 0.13791E-06).

The space group $P2_1$ was selected on the basis of systematic absences. The unique Mo atom was located by SHELX-S86 [20] and the remaining atoms were established by DIRDIF [18] structure programs and refined by full-matrix least-squares refinement. After

TABLE 2. Atomic positional parameters and equivalent isotropic displacement parameters (Å^2) and their e.s.d.s for $[Bu^n_4N]_4[Mo_2(CN)_8]\cdot 8CHCl_3$, ($\mathbf{1}\cdot 8CHCl_3$)

Atom	x	y	z	B_{eq}[a]
Mo(1)	0.96425(4)	0.00343(3)	0.03830(5)	2.34(4)
N(1)	0.8832(5)	0.1023(3)	−0.0001(5)	3.8(6)
N(2)	1.0378(6)	0.0679(4)	0.1573(5)	4.4(6)
N(3)	0.8336(5)	−0.0562(3)	−0.0166(5)	3.8(6)
N(4)	0.9818(5)	−0.0889(4)	0.1426(5)	3.9(6)
N(5)	0.3119(5)	0.0465(3)	0.7032(5)	3.6(5)
N(6)	0.0664(5)	0.1996(3)	0.0459(6)	4.6(6)
C(1)	0.9123(6)	0.0687(4)	0.0104(6)	2.7(6)
C(2)	1.0157(6)	0.0457(4)	0.1140(6)	2.9(6)
C(3)	0.8787(6)	−0.0356(4)	−0.0012(6)	2.7(6)
C(4)	0.9794(5)	−0.0593(4)	0.1053(6)	2.8(6)
C(5)	0.2988(6)	0.0357(4)	0.6311(6)	3.3(6)
C(6)	0.2310(6)	0.0508(5)	0.6090(7)	4.9(8)
C(7)	0.2250(6)	0.0429(4)	0.5302(8)	5.1(8)
C(8)	0.1568(7)	0.0554(5)	0.5022(8)	7(1)
C(9)	0.2611(7)	0.0237(5)	0.7506(8)	5.4(8)
C(10)	0.2544(8)	−0.0294(5)	0.7487(8)	6(1)
C(11)	0.204(1)	−0.0452(7)	0.800(2)	13(2)
C(12)	0.148(2)	−0.031(1)	0.793(2)	22(3)
C(13)	0.3803(6)	0.0270(4)	0.7170(7)	4.1(7)
C(14)	0.4049(8)	0.0300(5)	0.7908(7)	5.3(8)
C(15)	0.4766(7)	0.0129(6)	0.7951(8)	7(1)
C(16)	0.5002(9)	0.0137(7)	0.8664(8)	9(1)
C(17)	0.3106(6)	0.0996(5)	0.7174(6)	4.1(7)
C(18)	0.3544(6)	0.1295(5)	0.6739(7)	4.6(8)
C(19)	0.3459(8)	0.1823(5)	0.6903(7)	6(1)
C(20)	0.389(1)	0.2140(5)	0.6487(8)	8(1)
C(21)	0.0497(7)	0.2493(6)	0.026(1)	7(1)
C(22)	0.0004(7)	0.2576(5)	−0.025(1)	7(1)
C(23)	−0.019(1)	0.3082(7)	−0.041(2)	19(2)
C(24)	0.028(2)	0.341(1)	−0.040(3)	31(5)
C(25)	0.0073(6)	0.1734(4)	0.0737(7)	4.8(8)
C(26)	−0.026(1)	0.1950(6)	0.131(1)	11(1)
C(27)	−0.0768(8)	0.1628(6)	0.162(1)	9(1)
C(28)	−0.108(1)	0.185(1)	0.223(1)	20(2)
C(29)	0.1210(7)	0.2035(6)	0.0963(9)	6(1)
C(30)	0.1473(9)	0.1583(7)	0.1214(8)	7(1)
C(31)	0.205(2)	0.164(2)	0.179(2)	17(3)
C(32)	0.185(2)	0.179(2)	0.220(3)	36(6)
C(33)	0.0873(6)	0.1710(4)	−0.0157(7)	4.0(7)
C(34)	0.1438(6)	0.1926(5)	−0.0565(8)	5.0(8)
C(35)	0.1669(7)	0.1577(5)	−0.1113(7)	5.2(8)
C(36)	0.2206(8)	0.1796(6)	−0.1545(8)	8(1)
Cl(1)	1.1089(2)	0.1276(2)	0.6880(3)	11.4(4)
Cl(2)	1.0613(3)	0.2098(2)	0.7566(3)	11.1(4)
Cl(3)	0.9757(2)	0.1555(2)	0.6756(3)	9.5(3)
Cl(4)	0.3154(2)	0.2317(1)	0.4657(3)	9.7(3)
Cl(5)	0.2221(2)	0.1824(2)	0.5506(3)	8.7(3)
Cl(6)	0.2250(2)	0.1649(2)	0.4086(3)	8.8(3)
Cl(7)	0.3075(2)	0.1582(1)	0.0221(3)	8.0(3)
Cl(8)	0.3485(3)	0.0739(2)	0.0868(3)	10.2(4)
Cl(9)	0.3467(3)	0.0790(2)	−0.0559(3)	10.7(4)
Cl(10)	0.4603(5)	0.1124(3)	0.1759(4)	18.1(7)
Cl(11)	0.5964(4)	0.0974(3)	0.1631(4)	17.9(7)
Cl(12)	0.5475(5)	0.1866(3)	0.2054(5)	20.2(8)
C(37)	1.0444(8)	0.1510(5)	0.7296(8)	7(1)
C(38)	0.2701(7)	0.1787(5)	0.4812(9)	7(1)
C(39)	0.3080(7)	0.0973(5)	0.0149(8)	6(1)
C(40)	0.535(1)	0.129(1)	0.199(3)	46(5)
H(1)	0.3297	0.0521	0.6039	4.1
H(2)	0.3029	0.0025	0.6239	4.1
H(3)	0.1995	0.0322	0.6322	5.8
H(4)	0.2247	0.0835	0.6198	5.8
H(5)	0.2564	0.0623	0.5084	6.0
H(6)	0.2335	0.0104	0.5207	6.0
H(7)	0.1478	0.0881	0.5107	8.4
H(8)	0.1561	0.0500	0.4549	8.4
H(9)	0.1248	0.0363	0.5234	8.4
H(10)	0.2725	0.0322	0.7953	6.4
H(11)	0.2199	0.0368	0.7396	6.4
H(12)	0.2401	−0.0391	0.7052	7.4
H(13)	0.2952	−0.0439	0.7583	7.4
H(14)	0.2041	−0.0786	0.8022	15.1
H(15)	0.2185	−0.0330	0.8435	15.1
H(16)	0.1460	0.0027	0.7912	25.9
H(17)	0.1315	−0.0430	0.7502	25.9
H(18)	0.1202	−0.0424	0.8275	25.9
H(19)	0.3804	−0.0057	0.7043	5.1
H(20)	0.4100	0.0439	0.6895	5.1
H(21)	0.4026	0.0620	0.8056	6.3
H(22)	0.3785	0.0106	0.8186	6.3
H(23)	0.4791	−0.0190	0.7786	8.7
H(24)	0.5032	0.0328	0.7683	8.7
H(25)	0.4738	−0.0062	0.8931	10.9
H(26)	0.5441	0.0028	0.8675	10.9
H(27)	0.4984	0.0454	0.8826	10.9
H(28)	0.2671	0.1105	0.7110	4.8
H(29)	0.3230	0.1044	0.7629	4.8
H(30)	0.3986	0.1207	0.6818	5.5
H(31)	0.3441	0.1243	0.6278	5.5
H(32)	0.3017	0.1907	0.6823	7.2
H(33)	0.3558	0.1870	0.7365	7.2
H(34)	0.4332	0.2060	0.6564	10.3
H(35)	0.3789	0.2098	0.6023	10.3
H(36)	0.3816	0.2462	0.6609	10.3
H(37)	0.0358	0.2652	0.0657	8.7
H(38)	0.0891	0.2637	0.0104	8.7
H(39)	0.0146	0.2412	−0.0646	8.2
H(40)	−0.0386	0.2436	−0.0091	8.2
H(41)	−0.0148	0.3091	−0.0935	22.5
H(42)	−0.0578	0.3149	−0.0297	22.5
H(43)	0.0670	0.3394	−0.0399	33.6
H(44)	0.0079	0.3737	−0.0412	33.6
H(45)	0.0238	0.3453	0.0237	33.6
H(46)	−0.0236	0.1706	0.0385	5.8
H(47)	0.0213	0.1426	0.0871	5.8
H(48)	0.0060	0.2019	0.1648	13.0
H(49)	−0.0460	0.2234	0.1169	13.0
H(50)	−0.1100	0.1574	0.1294	10.7
H(51)	−0.0571	0.1335	0.1738	10.7
H(52)	−0.0746	0.1899	0.2570	24.0
H(53)	−0.1273	0.2140	0.2125	24.0
H(54)	−0.1393	0.1635	0.2416	24.0
H(55)	0.1560	0.2204	0.0758	7.3
H(56)	0.1055	0.2209	0.1340	7.3
H(57)	0.1126	0.1406	0.1409	8.2
H(58)	0.1647	0.1410	0.0843	8.2
H(59)	0.2232	0.1338	0.1886	20.2

(*continued*)

TABLE 2. (*continued*)

(*continued*)

TABLE 2. (*continued*)

Atom	x	y	z	B_{eq}[a]
H(60)	0.2383	0.1844	0.1616	20.2
H(61)	0.2180	0.1824	0.2545	42.1
H(62)	0.1668	0.2088	0.2110	42.1
H(63)	0.1520	0.1582	0.2381	42.1
H(64)	0.1005	0.1404	−0.0009	4.8
H(65)	0.0508	0.1681	−0.0448	4.8
H(66)	0.1293	0.2210	−0.0773	6.1
H(67)	0.1789	0.1993	−0.0270	6.1
H(68)	0.1832	0.1298	−0.0901	6.3
H(69)	0.1311	0.1497	−0.1392	6.3
H(70)	0.2569	0.1874	−0.1267	9.5
H(71)	0.2339	0.1574	−0.1878	9.5
H(72)	0.2048	0.2076	−0.1754	9.5
H(73)	1.0342	0.1316	0.7672	8.0
H(74)	0.3003	0.1536	0.4886	8.0
H(75)	0.2644	0.0861	0.0138	7.5
H(76)	0.5368	0.1151	0.2586	32.4

[a]Anisotropically refined atoms are given in the form of the isotropic equivalent thermal parameter defined as $4/3[a^2\beta_{11}+b^2\beta_{22}+c^2\beta_{33}+ab(\cos\gamma)\beta_{12}+ac(\cos\beta)\beta_{13}+bc(\cos\alpha)\beta_{23}]$.

all non-hydrogen atoms had been refined isotropically, an empirical absorption correction was applied using the program DIFABS [19]. Hydrogen atoms were included in the refinement in calculated positions. The final cycle of full matrix least-squares refinement was based on 3108 observed reflections with $F_o^2 > 3\sigma(F_o^2)$ and 497 variables to give $R = 0.067$ and $R_w = 0.067$ and a quality-of-fit index of 2.89. Both enantiomorphs were refined, but the difference in R values was not significant to any level of confidence by the Hamilton significance test, thereby precluding the assignment of one enantiomorph over the other.

*$[Bu^n_4N]_2[Re_2(CN)_6(dppm)_2]\cdot 8CH_2Cl_2$ (**4**·$8CH_2Cl_2$)*

Suitable crystals of $[Bu_4N]_2[Re_2(CN)_6(dppm)_2]\cdot 8CH_2Cl_2$ were obtained by slowly cooling a saturated CH_2Cl_2 solution of the compound. A crystal of dimensions $0.52\times0.26\times0.16$ mm was mounted on the end of a glass fiber with the aid of silicone grease. A least-squares refinement using the setting angles of 19 carefully centered reflections in the range $20 \leqslant 2\theta \leqslant 30°$ gave cell constants that correspond to a triclinic crystal system. A total of 10184 data was collected at a temperature of -100 ± 1 °C using the ω–2θ scan technique in the range $7 \leqslant 2\theta \leqslant 50°$ and was corrected for secondary extinction (coefficient = 0.86499E-07). The intensities of three representative reflections measured after every 150 reflections decayed by only 0.25%. An absorption correction based on three ψ-curves with a χ value near 90° was used and resulted in transmission factors ranging from 0.64 to 1.00.

TABLE 3. Atomic positional parameters and equivalent isotropic displacement parameters (Å^2) and their e.s.d.s for $[Bu^n_4N]_3[Mo_2(O_2CCH_3)(CN)_6]$ (**2**)

Atom	x	y	z	B_{eq}[a]
Mo(1)	0.0808(1)	0.2977	0.72110(7)	4.78(9)
Mo(2)	0.0710(1)	0.3948(2)	0.80504(7)	4.30(8)
O(1)	0.192(1)	0.229(1)	0.8005(7)	5.5(7)
O(2)	0.1786(9)	0.329(1)	0.8890(6)	5.3(7)
N(1)	−0.075(1)	0.339(1)	0.5566(8)	6(1)
N(2)	−0.132(2)	0.168(2)	0.745(1)	8(1)
N(3)	0.292(1)	0.355(2)	0.6167(9)	10(1)
N(4)	−0.092(1)	0.536(1)	0.712(1)	6(1)
N(5)	−0.121(1)	0.355(1)	0.9311(8)	5.3(9)
N(6)	0.290(1)	0.519(1)	0.800(1)	8(1)
N(7)	−0.404(1)	0.408(1)	0.7369(9)	5.7(9)
N(8)	0.098(2)	0.593(1)	0.016(1)	7(1)
N(9)	0.882(1)	0.062(2)	0.5054(8)	7(1)
C(1)	−0.021(1)	0.333(1)	0.6162(9)	5(1)
C(2)	−0.060(2)	0.214(2)	0.744(1)	5(1)
C(3)	0.223(1)	0.339(2)	0.655(1)	6(1)
C(4)	−0.037(2)	0.490(2)	0.743(1)	5(1)
C(5)	−0.061(1)	0.366(1)	0.8815(9)	4(1)
C(6)	0.213(2)	0.473(2)	0.793(1)	6(1)
C(7)	0.224(1)	0.263(2)	0.868(1)	5(1)
C(8)	0.301(2)	0.213(2)	0.923(1)	8(1)
C(9)	−0.350(1)	0.424(2)	0.822(1)	7(1)
C(10)	−0.435(2)	0.440(2)	0.884(1)	7(1)
C(11)	−0.370(2)	0.481(2)	0.957(1)	10.5(7)
C(12)	−0.451(2)	0.494(2)	1.018(2)	12.1(8)
C(13)	−0.307(1)	0.389(2)	0.686(1)	6(1)
C(14)	−0.341(2)	0.360(2)	0.603(2)	11(2)
C(15)	−0.337(3)	0.424(3)	0.551(2)	14(1)
C(16)	−0.345(3)	0.390(3)	0.459(2)	18(1)
C(17)	−0.480(1)	0.334(2)	0.738(1)	5(1)
C(18)	−0.428(2)	0.255(2)	0.768(1)	7(1)
C(19)	−0.508(2)	0.185(2)	0.754(1)	7.8(5)
C(20)	−0.473(2)	0.101(2)	0.787(1)	10.5(7)
C(21)	−0.470(2)	0.482(2)	0.706(1)	7(1)
C(22)	−0.408(2)	0.562(2)	0.702(1)	9(2)
C(23)	−0.492(3)	0.630(3)	0.678(2)	13(1)
C(24)	−0.438(3)	0.716(3)	0.682(2)	13(1)
C(25)	0.029(2)	0.604(2)	−0.058(1)	8(2)
C(26)	−0.021(3)	0.689(2)	−0.073(2)	15(2)
C(27)	−0.082(2)	0.703(2)	−0.154(1)	10.3(7)
C(28)	−0.184(2)	0.657(2)	−0.144(1)	11.0(7)
C(29)	0.023(2)	0.589(1)	0.085(1)	6(1)
C(30)	−0.072(2)	0.523(2)	0.085(2)	10(2)
C(31)	−0.112(3)	0.511(3)	0.164(2)	15(1)
C(32)	−0.197(6)	0.477(5)	0.173(4)	29(2)
C(33)	0.181(2)	0.658(1)	0.029(1)	8(1)
C(34)	0.259(2)	0.661(2)	−0.035(1)	9.2(6)
C(35)	0.348(2)	0.724(2)	−0.012(1)	10.2(7)
C(36)	0.427(2)	0.737(2)	−0.075(1)	11.2(7)
C(37)	0.145(2)	0.505(2)	0.012(1)	6(1)
C(38)	0.217(2)	0.476(2)	0.084(1)	9(1)
C(39)	0.268(2)	0.393(2)	0.076(1)	8.1(5)
C(40)	0.339(2)	0.371(2)	0.157(1)	9.5(6)
C(41)	0.865(2)	0.076(1)	0.417(1)	6(1)
C(42)	0.843(3)	0.166(2)	0.389(1)	11(2)
C(43)	0.838(2)	0.178(2)	0.311(2)	12.8(9)
C(44)	0.798(2)	0.263(2)	0.282(1)	10.2(7)
C(45)	0.787(2)	0.100(2)	0.547(1)	7(1)

(*continued*)

TABLE 3. (*continued*)

Atom	x	y	z	B_{eq}[a]
C(46)	0.675(2)	0.064(2)	0.518(1)	10(2)
C(47)	0.555(4)	0.120(4)	0.546(2)	21(2)
C(48)	0.574(5)	0.040(5)	0.595(3)	27(2)
C(49)	0.892(2)	−0.030(2)	0.519(1)	8(2)
C(50)	0.915(2)	−0.048(3)	0.608(2)	13(2)
C(51)	0.930(5)	−0.125(5)	0.625(3)	22(2)
C(52)	0.847(3)	−0.178(3)	0.607(2)	18(1)
C(53)	0.979(2)	0.109(2)	0.539(1)	7(1)
C(54)	1.093(2)	0.084(2)	0.508(1)	10(2)
C(55)	1.195(2)	0.133(2)	0.548(2)	10.9(8)
C(56)	1.203(3)	0.088(3)	0.629(3)	19(1)
H(1)	0.2686	0.2019	0.9737	11.8
H(2)	0.3310	0.1659	0.9039	11.8
H(3)	0.3665	0.2510	0.9411	11.8
H(4)	−0.2979	0.3793	0.8395	8.5
H(5)	−0.2994	0.4742	0.8222	8.5
H(6)	−0.4957	0.4716	0.8652	9.8
H(7)	−0.4637	0.3862	0.9035	9.8
H(8)	−0.3023	0.4537	0.9797	14.8
H(9)	−0.3396	0.5392	0.9439	14.8
H(10)	−0.4184	0.5217	1.0679	13.5
H(11)	−0.5128	0.5253	1.0004	13.5
H(12)	−0.4751	0.4402	1.0365	13.5
H(13)	−0.2605	0.4395	0.6827	8.0
H(14)	−0.2589	0.3475	0.7108	8.0
H(15)	−0.2902	0.3200	0.5826	12.7
H(16)	−0.4132	0.3388	0.5978	12.7
H(17)	−0.4021	0.4625	0.5555	18.4
H(18)	−0.2730	0.4601	0.5608	18.4
H(19)	−0.4079	0.3579	0.4480	19.5
H(20)	−0.3410	0.4342	0.4211	19.5
H(21)	−0.2788	0.3552	0.4534	19.5
H(22)	−0.5415	0.3453	0.7724	7.0
H(23)	−0.5163	0.3233	0.6859	7.0
H(24)	−0.3626	0.2389	0.7403	8.2
H(25)	−0.4056	0.2532	0.8238	8.2
H(26)	−0.5821	0.1961	0.7755	9.9
H(27)	−0.5315	0.1757	0.6956	9.9
H(28)	−0.5319	0.0580	0.7735	13.1
H(29)	−0.4103	0.0832	0.7603	13.1
H(30)	−0.4605	0.1038	0.8402	13.1
H(31)	−0.5014	0.4689	0.6532	8.9
H(32)	−0.5336	0.4879	0.7388	8.9
H(33)	−0.3775	0.5704	0.7573	10.6
H(34)	−0.3542	0.5553	0.6692	10.6
H(35)	−0.5200	0.6255	0.6248	15.4
H(36)	−0.5551	0.6329	0.7113	15.4
H(37)	−0.4203	0.7278	0.7381	16.4
H(38)	−0.3857	0.7205	0.6515	16.4
H(39)	−0.5010	0.7571	0.6678	16.4
H(40)	0.0840	0.5919	−0.1039	9.3
H(41)	−0.0236	0.5597	−0.0687	9.3
H(42)	−0.0664	0.7002	−0.0268	13.7
H(43)	0.0421	0.7327	−0.0604	13.7
H(44)	−0.0983	0.7602	−0.1686	12.1
H(45)	−0.0422	0.6796	−0.1969	12.1
H(46)	−0.2248	0.6796	−0.1016	13.3
H(47)	−0.2350	0.6551	−0.1909	13.3
H(48)	−0.1684	0.5989	−0.1295	13.3
H(49)	0.0662	0.5841	0.1378	9.0
H(50)	−0.0152	0.6446	0.0914	9.0
H(51)	−0.1355	0.5377	0.0504	13.1
H(52)	−0.0442	0.4701	0.0652	13.1
H(53)	−0.0536	0.4739	0.1937	16.3
H(54)	−0.1086	0.5614	0.1910	16.3
H(55)	−0.2618	0.5073	0.1522	30.6
H(56)	−0.2068	0.4199	0.1550	30.6
H(57)	−0.2138	0.4709	0.2327	30.6
H(58)	0.1365	0.7122	0.0268	11.9
H(59)	0.2150	0.6561	0.0807	11.9
H(60)	0.2960	0.6062	−0.0376	11.9
H(61)	0.2255	0.6718	−0.0863	11.9
H(62)	0.3050	0.7754	−0.0045	14.0
H(63)	0.3800	0.7086	0.0388	14.0
H(64)	0.4712	0.6854	−0.0805	13.2
H(65)	0.3965	0.7527	−0.1235	13.2
H(66)	0.4842	0.7783	−0.0560	13.2
H(67)	0.0856	0.4643	0.0004	9.5
H(68)	0.1892	0.5020	−0.0359	9.5
H(69)	0.2795	0.5150	0.0942	10.3
H(70)	0.1760	0.4769	0.1302	10.3
H(71)	0.2056	0.3530	0.0657	10.9
H(72)	0.3092	0.3911	0.0298	10.9
H(73)	0.2971	0.3730	0.2038	12.8
H(74)	0.3744	0.3168	0.1570	12.8
H(75)	0.4007	0.4109	0.1677	12.8
H(76)	0.9298	0.0542	0.3886	8.6
H(77)	0.8028	0.0413	0.3936	8.6
H(78)	0.7803	0.1841	0.4156	13.5
H(79)	0.9074	0.1975	0.4122	13.5
H(80)	0.8974	0.1635	0.2835	14.8
H(81)	0.7723	0.1415	0.2857	14.8
H(82)	0.8567	0.3034	0.3032	11.3
H(83)	0.7894	0.2714	0.2273	11.3
H(84)	0.7316	0.2815	0.3061	11.3
H(85)	0.7989	0.1024	0.6057	9.8
H(86)	0.7817	0.1626	0.5338	9.8
H(87)	0.6671	0.0547	0.4661	13.4
H(88)	0.6729	0.0060	0.5458	13.4
H(89)	0.5302	0.0222	0.6519	33.8
H(90)	0.5796	−0.0241	0.5817	33.8
H(91)	0.6559	0.0302	0.6389	33.8
H(92)	0.5649	0.1677	0.5733	22.9
H(93)	0.4894	0.1132	0.5157	22.9
H(94)	0.8234	−0.0582	0.4942	11.6
H(95)	0.9507	−0.0540	0.4856	11.6
H(96)	0.9821	−0.0203	0.6337	16.4
H(97)	0.8550	−0.0263	0.6420	16.4
H(98)	0.9782	−0.1353	0.5840	25.0
H(99)	0.9513	−0.1306	0.6726	25.0
H(100)	0.7926	−0.1756	0.6424	21.9
H(101)	0.8198	−0.1805	0.5539	21.9
H(102)	0.8863	−0.2342	0.6174	21.9
H(103)	0.9635	0.1705	0.5250	9.8
H(104)	0.9866	0.1095	0.5956	9.8
H(105)	1.1091	0.0276	0.5123	12.2
H(106)	1.0920	0.0949	0.4465	12.2
H(107)	1.2660	0.1421	0.5202	13.6
H(108)	1.1788	0.1983	0.5574	13.6
H(109)	1.1390	0.0860	0.6509	22.4
H(110)	1.2254	0.0293	0.6133	22.4
H(111)	1.2650	0.1060	0.6637	22.4

[a]Anisotropically refined atoms are given in the form of the isotropic equivalent thermal parameter defined as $4/3[a^2\beta_{11}+b^2\beta_{22}+c^2\beta_{33}+ab(\cos\gamma)\beta_{12}+ac(\cos\beta)\beta_{13}+bc(\cos\alpha)\beta_{23}]$.

TABLE 4. Atomic positional parameters and equivalent isotropic displacement parameters (Å^2) and their e.s.d.s for $[Bu^n_4N]_2$-$[Re_2(CN)_6(dppm)_2]\cdot 8CH_2Cl_2$ (**4**$\cdot 8CH_2Cl_2$)

Atom	*x*	*y*	*z*	B_{eq}[a]
Re(1)	1.02288(2)	0.08407(1)	1.00331(2)	1.68(1)
P(1)	1.0689(1)	0.0396(1)	0.8275(1)	1.94(5)
P(2)	0.9753(1)	0.1286(1)	1.1790(1)	1.91(5)
N(1)	1.1544(4)	−0.0209(3)	1.1368(5)	2.8(2)
N(2)	1.2275(4)	0.2155(3)	1.1191(5)	3.0(2)
N(3)	0.9342(4)	0.2307(3)	0.9269(5)	3.1(2)
N(4)	0.7039(4)	0.3272(3)	0.7869(5)	2.6(2)
C(1)	1.1113(5)	0.0207(4)	1.0882(6)	2.2(2)
C(2)	1.1545(5)	0.1683(3)	1.0796(6)	2.1(2)
C(3)	0.9642(5)	0.1777(4)	0.9526(6)	2.3(2)
C(4)	1.0082(5)	−0.0611(4)	0.7328(6)	2.1(2)
C(11)	1.2036(5)	0.0383(3)	0.8342(6)	2.0(2)
C(12)	1.2815(6)	0.0447(4)	0.9412(7)	2.5(2)
C(13)	1.3811(6)	0.0395(4)	0.9416(7)	2.8(2)
C(14)	1.4031(6)	0.0278(4)	0.8372(7)	3.2(3)
C(15)	1.3273(6)	0.0227(4)	0.7308(7)	3.2(3)
C(16)	1.2277(5)	0.0286(4)	0.7294(6)	2.7(2)
C(21)	1.0266(5)	0.0952(4)	0.7248(6)	2.1(2)
C(22)	0.9364(5)	0.0747(4)	0.6275(6)	2.7(2)
C(23)	0.9057(6)	0.1241(4)	0.5597(6)	3.2(3)
C(24)	0.9670(7)	0.1950(5)	0.5904(6)	3.4(3)
C(25)	1.0590(6)	0.2162(4)	0.6866(7)	3.7(3)
C(26)	1.0883(6)	0.1679(4)	0.7535(7)	3.1(3)
C(31)	1.0510(5)	0.2205(4)	1.2934(6)	2.1(2)
C(32)	1.0441(6)	0.2881(4)	1.2625(7)	3.0(2)
C(33)	1.1000(7)	0.3598(4)	1.3451(8)	3.8(3)
C(34)	1.1626(7)	0.3643(4)	1.4587(7)	4.1(3)
C(35)	1.1715(7)	0.2983(5)	1.4903(7)	4.3(3)
C(36)	1.1158(5)	0.2263(4)	1.4090(6)	3.0(3)
C(41)	0.8457(5)	0.1501(3)	1.1656(6)	2.2(2)
C(42)	0.7717(5)	0.1450(4)	1.0565(6)	2.4(2)
C(43)	0.6754(5)	0.1622(4)	1.0506(7)	2.9(2)
C(44)	0.6483(6)	0.1844(4)	1.1531(7)	3.2(3)
C(45)	0.7198(6)	0.1893(5)	1.2631(8)	3.9(3)
C(46)	0.8169(6)	0.1726(4)	1.2688(6)	3.2(3)
C(47)	0.6410(6)	0.3906(4)	0.7697(8)	3.2(3)
C(48)	0.5413(6)	0.3867(5)	0.7968(9)	3.9(3)
C(49)	0.4930(8)	0.4567(6)	0.785(1)	5.1(4)
C(50)	0.3940(8)	0.4580(7)	0.813(1)	6.2(4)
C(51)	0.7273(6)	0.3208(4)	0.9131(6)	2.7(2)
C(52)	0.7743(7)	0.3958(5)	1.0172(7)	3.5(3)
C(53)	0.7956(7)	0.3819(5)	1.1373(7)	4.3(3)
C(54)	0.8563(8)	0.4536(6)	1.2435(9)	5.1(4)
C(55)	0.6451(6)	0.2485(4)	0.6953(7)	2.9(3)
C(56)	0.7073(6)	0.1831(4)	0.6879(8)	3.8(3)
C(57)	0.6388(7)	0.1035(5)	0.6125(8)	3.8(3)
C(58)	0.5794(8)	0.0741(6)	0.680(1)	5.3(4)
C(59)	0.8064(6)	0.3482(5)	0.7710(7)	2.9(3)
C(60)	0.8001(6)	0.3516(5)	0.6468(7)	3.8(3)
C(61)	0.9029(7)	0.3902(5)	0.6523(8)	4.3(3)
C(62)	0.900(1)	0.3960(7)	0.530(1)	5.5(4)
Cl(1)	1.0697(2)	0.4335(1)	1.0633(2)	5.8(1)
Cl(2)	1.2294(2)	0.3862(1)	0.9669(3)	6.9(1)
C(63)	1.1348(6)	0.3571(5)	1.022(1)	5.0(4)
Cl(3)	0.4850(2)	0.3222(2)	0.0576(3)	6.8(1)
Cl(4)	0.3650(2)	0.2318(2)	−0.1923(3)	8.1(1)
C(64)	0.3908(8)	0.2401(5)	−0.040(1)	6.4(4)
Cl(5)	0.4572(2)	0.1381(2)	0.3056(3)	6.8(1)
Cl(6)	0.3572(2)	0.1434(2)	0.4839(2)	8.4(1)
C(65)	0.3390(7)	0.1323(6)	0.3323(8)	5.7(4)
Cl(7)	0.3541(4)	0.4439(3)	0.3571(5)	14.7(3)
Cl(8)	0.5195(7)	0.3562(3)	0.4095(6)	28.1(5)
C(66)	0.396(1)	0.3530(7)	0.363(2)	17(1)
H(1)	1.273(5)	0.053(4)	1.000(6)	2(1)
H(2)	1.435(4)	0.041(3)	1.008(5)	2(1)
H(3)	1.466(5)	0.023(4)	0.834(6)	3(1)
H(4)	1.345(5)	0.012(4)	0.659(6)	4(1)
H(5)	1.181(6)	0.029(4)	0.666(7)	4(2)
H(6)	0.887(4)	0.023(3)	0.607(5)	2(1)
H(7)	0.842(5)	0.112(4)	0.496(6)	3(1)
H(8)	0.949(5)	0.225(4)	0.546(6)	2(1)
H(9)	1.100(5)	0.274(4)	0.707(6)	3(1)
H(10)	1.151(7)	0.171(6)	0.809(9)	8(2)
H(11)	1.001(4)	0.287(3)	1.179(5)	1(1)
H(12)	1.088(6)	0.405(5)	1.321(8)	6(2)
H(13)	1.199(5)	0.413(4)	1.511(6)	3(1)
H(14)	1.209(5)	0.302(4)	1.560(7)	4(1)
H(15)	1.121(5)	0.180(4)	1.427(6)	3(1)
H(16)	0.782(5)	0.129(3)	0.984(6)	2(1)
H(17)	0.620(6)	0.158(4)	0.971(7)	6(2)
H(18)	0.587(5)	0.196(4)	1.146(6)	3(1)
H(19)	0.703(7)	0.207(6)	1.325(8)	7(2)
H(20)	0.868(5)	0.175(4)	1.355(6)	4(1)
H(21)	0.678(5)	0.440(4)	0.820(6)	2(1)
H(22)	0.627(4)	0.391(3)	0.686(5)	1(1)
H(23)	0.500(5)	0.340(4)	0.748(6)	3(1)
H(24)	0.554(5)	0.383(4)	0.878(7)	4(1)
H(25)	0.542(7)	0.515(6)	0.839(9)	8(2)
H(26)	0.456(6)	0.448(4)	0.699(7)	4(1)
H(27)	0.357(8)	0.500(6)	0.80(1)	9(1)
H(28)	0.342(7)	0.398(6)	0.759(8)	7(1)
H(29)	0.41(1)	0.470(7)	0.92(1)	13(1)
H(30)	0.666(5)	0.306(3)	0.921(5)	2(1)
H(31)	0.776(5)	0.280(4)	0.922(6)	3(1)
H(32)	0.837(6)	0.413(4)	1.021(6)	4(1)
H(33)	0.745(6)	0.447(5)	1.011(7)	5(2)
H(34)	0.748(7)	0.353(5)	1.152(8)	7(2)
H(35)	0.842(6)	0.332(5)	1.135(7)	6(2)
H(36)	0.872(8)	0.450(6)	1.31(1)	8(2)
H(37)	0.938(9)	0.475(6)	1.25(1)	11(2)
H(38)	0.825(7)	0.499(5)	1.236(8)	6(2)
H(39)	0.576(6)	0.237(5)	0.715(7)	6(2)
H(40)	0.621(4)	0.257(3)	0.620(5)	2(1)
H(41)	0.760(6)	0.197(4)	0.652(7)	5(2)
H(42)	0.744(6)	0.185(5)	0.768(8)	5(2)
H(43)	0.594(5)	0.104(4)	0.536(6)	3(1)
H(44)	0.676(5)	0.055(4)	0.596(6)	4(1)
H(45)	0.537(8)	0.118(6)	0.71(1)	10(2)
H(46)	0.529(6)	0.026(5)	0.629(7)	5(1)
H(47)	0.633(8)	0.063(6)	0.76(1)	10(2)
H(48)	0.832(5)	0.403(4)	0.826(6)	4(1)
H(49)	0.850(6)	0.307(5)	0.785(7)	7(2)
H(50)	0.781(5)	0.295(4)	0.582(7)	4(1)
H(51)	0.739(6)	0.383(5)	0.616(7)	6(2)
H(52)	0.905(6)	0.440(5)	0.708(8)	6(2)
H(53)	0.964(7)	0.354(5)	0.683(8)	7(2)
H(54)	0.963(8)	0.429(6)	0.54(1)	9(2)
H(55)	0.876(6)	0.348(5)	0.471(7)	5(1)

(*continued*)

TABLE 4. (*continued*)

(*continued*)

TABLE 4. (*continued*)

Atom	x	y	z	B_{eq}[a]
H(56)	0.848(8)	0.427(6)	0.50(1)	8(1)
H(59)	1.1676	0.3419	1.0908	6.0
H(60)	1.0875	0.3136	0.9605	6.0
H(61)	0.4149	0.1940	−0.0284	7.9
H(62)	0.3289	0.2440	−0.0228	7.9
H(63)	0.3042	0.1726	0.3111	6.5
H(64)	0.2971	0.0831	0.2820	6.5
H(65)	0.3653	0.3341	0.4064	17.8
H(66)	0.3695	0.3193	0.2770	17.8
H(57)	0.934(5)	−0.058(3)	0.704(5)	2(1)
H(58)	1.028(4)	−0.077(3)	0.667(5)	2(1)

[a]Anisotropically refined atoms are given in the form of the isotropic equivalent thermal parameter defined as $4/3[a^2\beta_{11}+b^2\beta_{22}+c^2\beta_{33}+ab(\cos\gamma)\beta_{12}+ac(\cos\beta)\beta_{13}+bc(\cos\alpha)\beta_{23}]$.

The structure was solved by MITHRIL [17] and DIRDIF [18] structure programs and refined by full-matrix least-squares refinement. All non-hydrogen atoms were refined with anisotropic thermal parameters with the exception of atoms in the CH_2Cl_2 interstitial solvent; hydrogen atoms were included in calculated positions. The final cycle of full-matrix least-squares refinement was based on 7767 observed reflections with $F_o^2 > 3\sigma(F_o^2)$ and 801 variable parameters to give $R = 0.041$ and $R_w = 0.045$ and a quality-of-fit index of 1.94.

$[Re_2(MeCN)_{10}][Mo_6O_{19}]_2 \cdot 4CH_3CN \cdot 2H_2O$ ($6 \cdot 4CH_3CN \cdot 2H_2O$)

Crystals of **6** were obtained as a solvate containing both CH_3CN and H_2O from slow diffusion of CH_3CN solutions of $[Re_2(MeCN)_{10}][BF_4]_4$ and $[Bu^n{}_4N]_2[Mo_6O_{19}]$. A green–blue crystal of dimensions $0.39 \times 0.26 \times 0.08$ mm was mounted on the end of a glass fiber with silicone grease and cooled to -100 ± 1 °C. A unit cell determination based on 15 reflections in the range $28 \leqslant 2\theta \leqslant 30°$ gave cell constants that corresponded to a monoclinic crystal system. A total of 6736 reflections was collected of which 6508 were unique using an ω–2θ scan motion in the range $6 \leqslant 2\theta \leqslant 50°$. During data collection, the intensities of three representative reflections measured every 97 reflections revealed a significant decay of 60% in spite of the low temperature data collection; a linear correction factor was applied to correct for this phenomenon. Azimuthal scans of 3 reflections with Eulerian angle χ near 90° were used as a basis for an empirical absorption correction; transmission factors ranged from 0.46 to 1.00.

The space group was determined to be $C2/c$ on the basis of systematic absences. The positions of the Mo and Re atoms were located and the remaining structure was fully developed using the program DIRDIF [18].

TABLE 5. Atomic positional parameters and equivalent isotropic displacement parameters (Å^2) and their e.s.d.s for $[Re_2(MeCN)_{10}][Mo_6O_{19}]_2 \cdot 4CH_3CN \cdot 2H_2O$ ($6 \cdot 4CH_3CN \cdot 2H_2O$)

Atom	x	y	z	B_{eq}[a]
Re(1)	0.06146(7)	0.31672(5)	0.75304(8)	1.91(6)
Mo(1)	0.1312(2)	0.1067(1)	0.8735(2)	3.2(2)
Mo(2)	0.2844(2)	0.1355(1)	0.7862(2)	3.4(2)
Mo(3)	0.2212(2)	0.0002(1)	0.7900(2)	4.0(2)
Mo(4)	0.3660(2)	0.0349(1)	0.8896(2)	4.2(2)
Mo(5)	0.2760(2)	0.1410(1)	0.9744(2)	3.7(2)
Mo(6)	0.2119(2)	0.0062(1)	0.9770(2)	4.4(2)
O(1)	0.248(1)	0.0697(7)	0.880(1)	3(1)
O(2)	0.185(1)	0.1529(8)	0.797(1)	3(1)
O(3)	0.301(1)	0.182(1)	0.879(1)	4(1)
O(4)	0.196(1)	−0.0374(8)	0.885(1)	4(1)
O(5)	0.318(1)	−0.014(1)	0.810(1)	4(1)
O(6)	0.308(1)	0.185(1)	0.723(1)	5(1)
O(7)	0.122(1)	0.047(1)	0.950(1)	3(1)
O(8)	0.133(1)	0.048(1)	0.803(1)	4(1)
O(9)	0.045(1)	0.135(1)	0.868(1)	3.8(5)
O(10)	0.367(1)	0.096(1)	0.968(1)	5(1)
O(11)	0.373(1)	0.090(1)	0.810(1)	4(1)
O(12)	0.256(1)	0.068(1)	0.733(1)	4(1)
O(13)	0.175(1)	0.1568(9)	0.949(1)	3(1)
O(14)	0.204(1)	−0.048(1)	0.723(1)	6(2)
O(15)	0.449(1)	0.004(1)	0.896(2)	5(1)
O(16)	0.186(1)	−0.040(1)	1.045(2)	6.2(7)
O(17)	0.243(1)	0.075(1)	1.039(1)	5(1)
O(18)	0.297(1)	0.189(1)	1.044(1)	7(2)
O(19)	0.315(1)	−0.0146(9)	0.963(1)	5(1)
N(1)	0.075(1)	0.399(1)	0.804(1)	2.4(5)
N(2)	0.062(1)	0.283(1)	0.860(1)	2.3(5)
N(3)	0.076(1)	0.236(1)	0.702(1)	2.6(5)
N(4)	0.076(1)	0.352(1)	0.639(1)	2.5(5)
N(5)	0.197(1)	0.317(1)	0.773(2)	3.4(6)
C(1)	0.091(2)	0.440(1)	0.826(2)	2.8(7)
C(2)	0.112(2)	0.492(2)	0.853(3)	7(1)
C(3)	0.064(2)	0.268(1)	0.922(2)	2.2(6)
C(4)	0.056(2)	0.245(1)	1.000(2)	2.9(7)
C(5)	0.095(2)	0.192(1)	0.672(2)	2.4(6)
C(6)	0.119(2)	0.141(1)	0.639(2)	3.0(7)
C(7)	0.080(2)	0.369(1)	0.578(2)	3.2(7)
C(8)	0.081(2)	0.382(1)	0.502(2)	4.1(8)
C(9)	0.253(2)	0.317(1)	0.795(2)	3.3(7)
C(10)	0.323(2)	0.318(1)	0.825(2)	3.3(7)
O(20)	0.491(2)	0.198(2)	0.708(2)	12(1)
N(6)	0.858(3)	0.253(2)	−0.016(3)	12(1)
C(11)	0.8384	0.2223	0.0257	8(1)
C(12)	0.8012	0.1878	0.1041	10(1)
N(7)	0.0272	0.0312	0.1050	13(1)
C(13)	0.0080	0.0788	0.0958	16(2)
C(14)	−0.0163	0.1388	0.0841	42(5)
H(1)	0.1318	0.4899	0.9049	6.5
H(2)	0.1490	0.5108	0.8223	6.5
H(3)	0.0717	0.5200	0.8557	6.5
H(4)	0.0177	0.2651	1.0259	3.3
H(5)	0.0453	0.2038	0.9992	3.3
H(6)	0.1003	0.2507	1.0286	3.3
H(7)	0.0803	0.1196	0.6142	3.2
H(8)	0.1557	0.1485	0.6007	3.2
H(9)	0.1410	0.1142	0.6760	3.2
H(10)	0.1050	0.4195	0.4928	4.6
H(11)	0.1084	0.3528	0.4734	4.6
H(12)	0.0336	0.3840	0.4809	4.6
H(13)	0.3233	0.3143	0.8802	3.7
H(14)	0.3525	0.2871	0.8048	3.7
H(15)	0.3470	0.3551	0.8134	3.7

[a]Anisotropically refined atoms are given in the form of the isotropic equivalent thermal parameter defined as $4/3[a^2\beta_{11}+b^2\beta_{22}+c^2\beta_{33}+ab(\cos\gamma)\beta_{12}+ac(\cos\beta)\beta_{13}+bc(\cos\alpha)\beta_{23}]$.

TABLE 6. Atomic positional parameters and equivalent isotropic displacement parameters (Å²) and their e.s.d.s for $[Rh_2(MeCN)_{10}][Mo_6O_{19}]_2 \cdot 4CH_3CN$ ($7 \cdot 4CH_3CN$)

Atom	x	y	z	B_{eq}[a]
Rh(1)	0.07077(8)	0.31609(6)	0.2542(1)	1.76(7)
N(1)	0.073(1)	0.3958(7)	0.299(1)	2.2(9)
N(2)	0.062(1)	0.2824(7)	0.360(1)	2(1)
N(3)	0.1863(9)	0.3166(8)	0.266(1)	2.5(9)
N(4)	0.074(1)	0.2365(7)	0.207(1)	2(1)
N(5)	0.076(1)	0.3489(7)	0.148(1)	3(1)
C(1)	0.075(1)	0.3645(9)	0.085(1)	3(1)
C(2)	0.087(1)	0.440(1)	0.323(1)	3(1)
C(3)	0.059(1)	0.2661(9)	0.422(2)	3(1)
C(4)	0.247(1)	0.3155(9)	0.287(1)	4(1)
C(5)	0.089(1)	0.1940(9)	0.177(1)	3(1)
C(6)	0.112(1)	0.4977(9)	0.361(1)	4(1)
C(7)	0.053(1)	0.2441(9)	0.505(1)	3(1)
C(8)	0.326(1)	0.315(1)	0.316(1)	3.7(5)
C(9)	0.112(1)	0.1387(8)	0.137(1)	3(1)
C(10)	0.069(1)	0.384(1)	0.001(1)	3.9(5)
Mo(1)	0.3673(1)	0.39268(8)	0.6253(1)	3.0(1)
Mo(2)	0.2229(1)	0.35835(8)	0.5249(1)	3.6(1)
Mo(3)	0.2793(1)	0.50043(8)	0.7090(1)	3.7(1)
Mo(4)	0.2144(1)	0.36576(8)	0.7147(1)	3.3(1)
Mo(5)	0.1348(1)	0.46583(9)	0.6085(1)	3.9(1)
Mo(6)	0.2875(1)	0.49224(9)	0.5181(1)	3.9(1)
O(1)	0.2508(7)	0.4289(5)	0.6155(7)	1.8(6)
O(2)	0.1798(9)	0.5151(6)	0.686(1)	4(1)
O(3)	0.1317(8)	0.4044(6)	0.5336(8)	3.6(8)
O(4)	0.1268(8)	0.4077(6)	0.6893(9)	3.9(8)
O(5)	0.1876(9)	0.5119(6)	0.532(1)	4(1)
O(6)	0.202(1)	0.3071(7)	0.455(1)	5(1)
O(7)	0.302(1)	0.5497(6)	0.777(1)	6(1)
O(8)	0.451(1)	0.3647(6)	0.631(1)	5(1)
O(9)	0.2451(8)	0.4339(6)	0.7715(8)	3.4(8)
O(10)	0.313(1)	0.5401(7)	0.447(1)	6(1)
O(11)	0.3042(9)	0.5371(5)	0.6132(8)	3.8(8)
O(12)	0.2557(8)	0.4239(6)	0.4614(8)	3.6(8)
O(13)	0.1948(8)	0.3211(5)	0.6218(8)	3.6(8)
O(14)	0.186(1)	0.3179(7)	0.7850(9)	5(1)
O(15)	0.3222(8)	0.3427(6)	0.5471(8)	3.2(8)
O(16)	0.052(1)	0.4943(8)	0.602(1)	7(1)
O(17)	0.3150(8)	0.3462(5)	0.7012(8)	3.0(8)
O(18)	0.3748(8)	0.4501(6)	0.5439(9)	3.9(9)
O(19)	0.3693(8)	0.4548(6)	0.701(1)	3.9(8)
N(6)	0.639(2)	0.252(1)	0.500(2)	10(2)
C(11)	0.672(2)	0.281(1)	0.462(2)	6.2(8)
C(12)	0.702(2)	0.319(1)	0.408(2)	7.8(8)
N(7)	0.0187	0.0307	0.6233	13(1)
C(13)	−0.0073	0.0714	0.5946	22(2)
C(14)	−0.018(3)	0.128(2)	0.640(3)	18(2)

[a]Anisotropically refined atoms are given in the form of the isotropic equivalent thermal parameter defined as $4/3[a^2\beta_{11} + b^2\beta_{22} + c^2\beta_{33} + ab(\cos\gamma)\beta_{12} + ac(\cos\beta)\beta_{13} + bc(\cos\alpha)\beta_{23}]$.

The final cycle of full-matrix least-squares refinement was based on 2805 observed reflections $F_o^2 > 3\sigma(F_o^2)$ and 298 variables for a data-to-parameter ratio of 9.1. The refinement converged with residuals of $R = 0.066$ and $R_w = 0.083$ and a quality-of-fit index of 2.56. The largest shift/esd in the final cycle was 0.13.

$[Rh_2(MeCN)_{10}][Mo_6O_{19}]_2 \cdot 4CH_3CN$ ($7 \cdot 4CH_3CN$)

Suitable crystals of **7** were obtained as the CH_3CN solvate from a layer reaction of separate CH_3CN solutions of $[Rh_2(MeCN)_{10}][BF_4]_4$ and $[Bu^n_4N]_2[Mo_6O_{19}]$. An orange crystal of dimensions $0.96 \times 0.10 \times 0.07$ mm was mounted on the end of a glass fiber with viscous oil and cooled to -75 ± 1 °C in a nitrogen cold stream. Cell parameters determined from 25 reflections in the range $40 \leqslant 2\theta \leqslant 60°$ indicated a monoclinic crystal system which was confirmed by axial photography. Data were collected in the range $4 \leqslant 2\theta \leqslant 114°$ by an ω-scan motion with Cu Kα radiation. Three standard reflections measured every 100 reflections exhibited no significant decay in intensity over the duration of the data collection. An empirical absorption correction based on ψ-scans of three reflections with χ near 90° gave transmission factors from 0.39 to 1.00.

The space group was determined to be *C2/c* on the basis of systematic absences. The positions of the heavy atoms were located by DIRDIF [18]; a sequence of successive difference Fourier maps and least-squares cycles led to the location of the remaining non-hydrogen atoms. The final full-matrix refinement involved 389 variable parameters and 3772 observed reflections with $F_o^2 > 3\sigma(F_o^2)$ for a data-to-parameter ratio of 9.7. The refinement converged with residuals $R = 0.079$ and $R_w = 0.051$ and goodness-of-fit of 3.90.

Powder X-ray crystallography

A powder diffraction pattern of the desolvated oxide material, **14**, obtained from thermal treatment of $[Mo_2(MeCN)_{10}][Mo_6O_{19}]_2$ (**10**), was recorded on a Rigaku Rotoflex diffractometer. The Cu K_α and Cu K_β lines were obtained from a rotating Cu anode (45 kV, 100 mA) and collimated using a 1/6° scattering slit and a 1/6° receiving slit. The K_β line was removed by a curved graphitc single crystal monochromator (0.45° receiving slit and 0.45 mm monochromator). The sample was mounted by pressing dried powder on double-sided tape attached to a $1 \times 2''$ glass microscope slide. The resulting data were recorded and processed using the manufacturer provided software DMAXB on a microVAX computer.

Results and discussion

Synthesis of cyanide compounds from carboxylate and chloride compounds

In spite of the rich chemistry involving the cyanide ligand [21], the preparation of low valent cyanide complexes with metals that form strong M–M interactions has not been pursued to any great extent. With the exception of $[Et_4N]_4[Mo_2(CN)_8]$, formulated on the basis

of IR and elemental data [22], there are no reports of homoleptic dinuclear cyanide compounds in the literature to our knowledge. We wondered if the lack of activity in this area was due to the fact that metal–metal bond chemistry is typically performed in non-aqueous solvents whereas classical cyanide chemistry is carried out under aqueous conditions or in liquid ammonia. To test this assumption, we recently initiated a program aimed at synthesizing cyanide and mixed ligand cyanide compounds beginning with dinuclear starting materials and organic-soluble forms of CN^-. Substitution reactions of dimolybdenum tetracarboxylates with $[R_4N]CN$ (R = Et, Bu^n) were found to proceed rapidly in organic media to give $[Bu^n{}_4N]_4[Mo_2(CN)_8]\cdot 8CHCl_3$ (**1**) and $[Bu^n{}_4N]_3[Mo_2(O_2CCH_3)(CN)_6]$ (**2**). Chemistry of $Mo_2(O_2CR)_4$ (R = CH_3 or CF_3) with eight equivalents of $[Bu^n{}_4N]CN$ or $[Et_4N]CN$ in CH_2Cl_2 produces the blue octacyanide anion $[Mo_2(CN)_8]^{4-}$, with the highest yield obtained from $[Et_4N]CN$ and $Mo_2(O_2CCH_3)_4$. Substitutions involving $[Bu_4N]CN$ are less desirable, as these reactions invariably lead to intractable oily products contaminated with the purple intermediate $[Bu^n{}_4N]_3[Mo_2(O_2CCH_3)(CN)_6]$ (**2**). The anion in **2**, $[Mo_2(O_2CCH_3)(CN)_6]^{3-}$, was rationally prepared by reaction of six equivalents of $[Bu^n{}_4N]CN$ with $Mo_2(O_2CCH_3)_4$ in THF and subsequently converted to $[Mo_2(CN)_8]^{4-}$ by addition of $[Bu^n{}_4N]CN$ to a solution of the compound in CH_2Cl_2. The final product is difficult to isolate as the $[Bu^n{}_4N]^+$ salt, but it can be precipitated as $[Et_4N]_4[Mo_2(CN)_8]$ when treated with $[Et_4N]Cl$. Attempts to prepare the mono- or bis-substituted anions $[Mo_2(O_2CCH_3)_3(CN)_2]^-$ and $[Mo_2(O_2CCH_3)_2(CN)_4]^{2-}$ by an analogous procedure produced only mixtures of $[Bu^n{}_4N]_3[Mo_2(O_2CCH_3)(CN)_6]$ and $Mo_2(O_2CCH_3)_4$ as judged by NMR spectroscopic monitoring of reactions performed in deuterated solvents.

As part of the generality of our approach, we sought to demonstrate that Cl^- ligands of multiply-bonded compounds also readily exchange with CN^- in non-aqueous solvents. The reaction of purple $Re_2Cl_4(dppm)_2$ with excess CN^- in toluene or CH_2Cl_2 proceeds at ambient temperatures with precipitation of green $[Bu^n{}_4N]_2[Re_2(CN)_6(dppm)_2]$ (**4**), the first example of a M–M bonded anion of the type $[M_2L_{10}]^{2-}$. No evidence for the formation of partially substituted compounds or the simple adduct $[Re_2Cl_4(CN)_2(dppm)_2]^{2-}$ was observed. $[Re_2(CN)_6(dppm)_2]^{2-}$ is quite stable in air, and, indeed, is inert to CO under prolonged reflux conditions in CH_2Cl_2, which underscores the stability of this dinuclear unit supported by six cyanide ligands.

Synthesis of salts containing solvated dinuclear cations

We have found that protonation of the ligands in $Re_2Cl_4(PPr^n{}_3)_4$ with HBF_4 in CH_3CN/CH_2Cl_2 provides a high yield route into the hitherto unknown triply-bonded cation $[Re_2(MeCN)_{10}]^{4+}$. The compound can also be prepared from $[Re_2Cl_8]^{2-}$ and HBF_4, but this chemistry involves reduction of the dirhenium unit and produces only low yields of the solvated Re_2^{4+} cation [4]. Both reactions are quite surprising, as they involve replacement of the excellent stabilizing ligands Cl^- and PR_3 with a nitrile, a somewhat counterintuitive reaction. A driving force for these processes is the liberation of volatile HCl and stable phosphonium cations $[HPR_3]^+$ neither of which can easily back-react with the solvated cation. The success of the reaction is also dependent on the addition of CH_2Cl_2 to the reaction mixture to induce precipitation of the product during the course of the reaction. This synthetic approach may prove to be very useful for a variety of applications in transition metal chemistry, especially for the mild substitution of phosphine ligands.

The preparative strategy for the polyoxometallate salts containing dinuclear cations is metathetic replacement of the $[BF_4]^-$ anion in the soluble salts $[M_2(MeCN)_{10}][BF_4]_4$ with $[M_6O_{19}]^{2-}$ or $[Mo_8O_{26}]^{4-}$ in CH_3CN to give the insoluble 1:2 salts $[M_2(MeCN)_{10}][X]_2$ (X = $[M_6O_{19}]^{2-}$; M = Mo, W) or the 1:1 salts $[M_2(MeCN)_{10}][Mo_8O_{26}]$. Our original goal in preparing these compounds was to seek higher quality crystals of the solvated dinuclear cations, as we and others had observed that they tend to form disordered structures with $[BF_4]^-$ anions. For example, efforts in our laboratories to structurally characterize $[Re_2(MeCN)_{10}][BF_4]_4$ met with repeated failure due to a three-fold disorder of the Re_2 unit in the body-centered cubic lattice. The structures of the Mo and Rh analogues also suffer somewhat from low crystal quality. In contemplating the choice of another anion, we were sensitive to the issue of reactivity, as many anions behave as good nucleophiles for electrophilic metal centers. Polyoxometallates of the type used in this study are good choices because of their solubility as $[Bu^n{}_4N]^+$ salts and their inert behavior. Judging by the ease with which the salts **6–12** crystallized, it appears that metal oxide anions are excellent choices for the convenient isolation and crystallization of large, reactive inorganic cations.

Spectroscopic measurements

The electronic spectra of $[Mo_2(CN)_8]^{4-}$ and $[Mo_2(O_2CCH_3)(CN)_6]^{3-}$ exhibit transitions in the visible region characteristic of $\delta \rightarrow \delta^*$ transitions at λ_{max} values of 601 and 557 nm, respectively. The value for the octacyanide complex is considerably lower in energy than the corresponding transitions in homoleptic quadruply-bonded Mo_2^{4+} compounds with halide ligands, e.g. $[Mo_2Cl_8]^{4-}$ exhibits a δ–δ^* transition at 530 nm [23]. Clearly the energy separation of the δ and δ^* molecular orbitals is considerably smaller in the presence

of cyanide ligands acting as strong donors. The IR spectrum of $(Bu_4N)_4[Mo_2(CN)_8]$ reveals two $\nu(C\equiv N)$ stretches at 2095 and 2103 cm^{-1} in the solid state and one stretch at 2096 cm^{-1} in CH_2Cl_2 solution. The high energies of the cyanide stretches indicate that the cyanide groups are acting solely as donors and not as π acceptors. The anion $[Mo_2(O_2CCH_3)(CN)_6]^{3-}$ exhibits $\nu(C\equiv N)$ stretches at 2099 and 2105 cm^{-1} for two distinct types of $C\equiv N^-$ in a C_{2v} symmetry environment. As in $[Mo_2(CN)_8]^{4-}$, these stretching frequencies are higher than free CN^- for which $\nu(C\equiv N)$ occurs at 2050 cm^{-1} in $[Bu^n_4N]CN$. The ^1H NMR spectrum of $[Bu^n_4N]_4Mo_2(CN)_8]$ in CD_2Cl_2 displays only resonances at $\delta = 0.98$, 1.49, 1.72, 3.42 ppm (3:2:2:2 integration) for the butyl substituents of the $[Bu^n_4N]^+$ groups. For $[Bu^n_4N]_3[Mo_2(O_2CCH_3)(CN)_6]$, the ^1H NMR spectrum in $CDCl_3$ exhibits a singlet at $\delta = 2.60$ ppm for the methyl group of (μ-O_2CCH_3) in addition to the $[Bu^n_4N]^+$ resonances at $\delta = 0.92$, 1.47, 1.68, 3.36 ppm (3:2:2:2 integration).

$[Bu^n_4N]_2[Re_2(CN)_6(dppm)_2]$; (**4**) displays $\nu(C\equiv N)$ stretches indicative of terminal (2097 and 2081 cm^{-1}) and bridging cyanide ligands (1935 cm^{-1}). The compound exhibits very low solubility in nearly all solvents except CH_3CN, in which it is sufficiently soluble to allow for solution measurements. A $^{31}P\{1H\}$ spectrum of **4** recorded in CD_3CN at 22 °C relative to 85% H_3PO_4 contained a singlet at −11.39 ppm which is in the range of chemical shifts observed for Re_2^{4+} complexes containing *trans* dppm ligands [24]. ^1H NMR spectral properties of the anion are typical for symmetrical bis-dppm complexes of Re(II): ^1H NMR (CD_3CN, 22 °C, 300 MHz): δ 7.48 (mult, 16H, Ph); 6.96 (mult, 24H, Ph); 5.44 (s, 16H, CH_2Cl_2); 3.30 (pentet, 4H, $-CH_2-$). The pentet for the methylene bridgehead group arises from four equivalent methylene protons undergoing virtual coupling with four equivalent P nuclei (J(P–H) = 3.9 Hz). Electronic d–d transitions for $[Re_2(CN)_6(dppm)_2]^{2-}$ occur at 969 and 694 with ϵ values in the $1\text{–}2\times10^2$ range. Since no other unambiguous examples of an Re_2^{4+} unit in an edge-sharing bioctahedral (ESBO) geometry exist, these transitions cannot be assigned by analogy to other systems. Electrochemical studies of **4** in CH_3CN revealed that the anion does not undergo any redox processes in the range +1.8 to −1.8 V versus Ag/AgCl. In contrast, Re_2^{4+} complexes of the M_2L_8 type ($\sigma^2\pi^4\delta^2\delta^{*2}$) exhibit two reversible or quasi-reversible oxidations corresponding to loss of the δ^* electrons [24, 25]. The situation is quite different in the present case, however, as the orbital overlap scheme of an ESBO compound places the last two electrons in a π^* level i.e. $\sigma^2\pi^2(\delta^2\delta^{*2})\pi^{*2}$. There is, therefore, no justification for correlating redox properties for the two different geometries.

The new polyoxometallate compounds isolated in this work were spectroscopically characterized by the signature vibrations of the individual ions, and by a comparison of their electronic properties to the corresponding properties of the $[M_2(MeCN)_{10}]^{4+}$ and $[Mo_6O_{19}]^{2-}$ chromophores in the original salts. Evidence for exchange of $[BF_4]^-$ for $[M_6O_{19}]^{2-}$ and $[Mo_8O_{26}]^{4-}$ in these compounds was obtained from IR spectra that reveal the characteristic $\nu(C\equiv N)$ and $\nu(M\text{–}O)$ stretches of the intact ions. IR data for the products **6–12** in the $\nu(M\text{–}O)$ region reveal the expected anion-dependent shifts of these vibrational modes as compared to the $[Bu^n_4N]^+$ salts [26]. The electronic absorption spectra of the $[Mo_6O_{19}]^{2-}$ compounds **6**, **7** and **10** in dimethylacetamide (DMAA) solutions exhibit the characteristic LMCT transition at 324 nm associated with the $[Mo_6O_{19}]^{2-}$. For the Re (**6**) and Rh (**7**) compounds, the d–d spectral features in the visible region are qualitatively similar to those of the $[BF_4]^-$ compounds, suggesting that the cation is stable in solution with respect to redox reactions with the oxoanion. In contrast, the Mo compound **10** undergoes rapid decomposition in DMAA judging by a rapid color change from blue to green and the appearance of an optical transition at 718 nm. For a complete listing of spectral data for the seven salts reported in this paper, see 'Experimental'.

Molecular structures

*$[Bu_4N]_4[Mo_2(CN)_8]\cdot 8CHCl_3$ (**1**$\cdot 8CHCl_3$)*

The structure of $[Bu^n_4N]_4[Mo_2(CN)_8]\cdot 8CHCl_3$ constitutes the first crystallographically determined dinuclear homoleptic cyanide complex. An ORTEP diagram of the molecular anion is depicted in Fig. 1. A list of selected bond distances and angles for the compound is given in Table 7. This anion constitutes an important

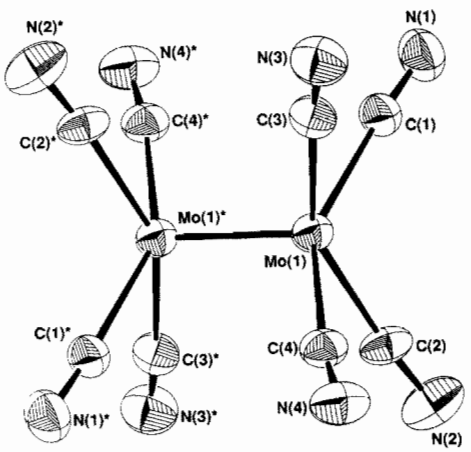

Fig. 1. ORTEP depiction of the molecular anion $[Mo_2(CN)_8]^{4-}$ with atoms represented by their 50% probability ellipsoids.

TABLE 7. Selected bond distances (Å) and bond angles (°) and their e.s.d.s for $[Bu^n_4N]_4[Mo_2(CN)_8]\cdot 8CHCl_3$ (**1**·$8CHCl_3$)

Bond distances			
Mo(1)–Mo(1)*	2.122(2)		
Mo(1)–C(1)	2.19(1)		
Mo(1)–C(2)	2.19(1)		
Mo(1)–C(3)	2.21(1)		
Mo(1)–C(4)	2.23(1)		
N(1)–C(1)	1.14(1)		
N(2)–C(2)	1.15(1)		
N(3)–C(3)	1.14(1)		
N(4)–C(4)	1.12(1)		
Bond angles			
Mo(1)*–Mo(1)–C(1)	103.4(3)	C(2)–Mo(1)–C(3)	153.6(4)
Mo(1)*–Mo(1)–C(2)	102.0(3)	C(2)–Mo(1)–C(4)	87.3(4)
Mo(1)*–Mo(1)–C(3)	104.4(3)	C(3)–Mo(1)–C(4)	85.9(4)
Mo(1)*–Mo(1)–C(4)	105.0(3)	Mo(1)–C(1)–N(1)	175(1)
C(1)–Mo(1)–C(2)	87.4(4)	Mo(1)–C(2)–N(2)	174(1)
C(1)–Mo(1)–C(3)	86.6(4)	Mo(1)–C(3)–N(3)	175(1)
C(1)–Mo(1)–C(4)	151.6(4)	Mo(1)–C(4)–N(4)	173(1)

TABLE 8. Comparison of the M–M bond distances in selected quadruply-bonded dimolybdenum complexes

Compound	Mo–Mo distance (Å)	Reference
$[Bu^n_4N]_4[Mo_2(CN)_8]\cdot 8CHCl_3$	2.122(2)	this paper
$[Bu^n_4N]_3[Mo_2(O_2CCH_3)(CN)_6]$	2.114(2)	this paper
$K_4Mo_2Cl_8$	2.139(4)	27
$[NH_4]_4[Mo_2(NCS)_8]\cdot 4H_2O$	2.162(1)	15a
$[Mo_2(MeCN)_{10}][BF_4]_4\cdot 2MeCN$	2.187(1)	8
$Mo_2(O_2CCH_3)_4$	2.0934(8)	28

example of an unsupported metal–metal quadruple bond in the presence of π-acceptor ligands. For comparative purposes, the Mo–Mo distances of unsupported homoleptic dimolybdenum compounds are listed in Table 8 along with those of compounds **1** and **2**. Among the unbridged compounds in this list, $[Mo_2(CN)_8]^{4-}$ possesses the shortest M–M interaction, a rather surprising finding, as π-acceptor CN^- ligands would be expected to produce the opposite effect. As the IR data in the $\nu(C\equiv N)$ region indicated, the ligands in compound **1** appear to be serving purely as donors for the Mo_2^{4+} core, thereby increasing the electron density at the metal centers and therefore improving M–M overlap. Other important metric parameters are Mo–C_{av} = 2.21, C–N_{av} = 1.14 Å, ⟨Mo–Mo–C_{av} = 103.7 and ⟨Mo–C–N_{av} = 174°; all are within expected ranges.

$[Bu^n_4N]_3[Mo_2(O_2CCH_3)(CN)_6]$ (2)

The structure of $[Bu^n_4N]_3[Mo_2(O_2CCH_3)(CN)_6]$ is unusual in that the anion possesses only one bridging acetate group, a situation that is rarely encountered [29]. As the ORTEP in Fig. 2 clearly shows, the molecular

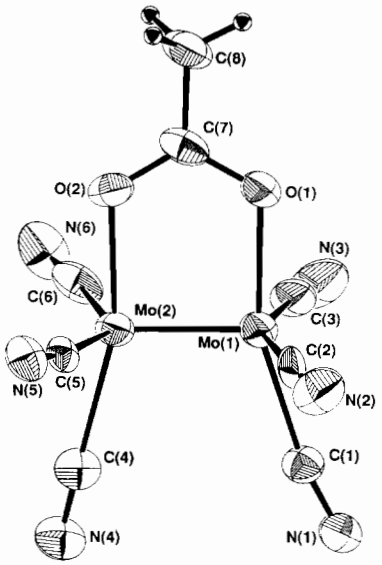

Fig. 2. Molecular structure of $[Mo_2(O_2CCH_3)(CN)_6]^{3-}$, with the atom labeling scheme. With the exception of the H atoms, the atoms are represented by their 50% probability ellipsoids.

anion approximates an eclipsed M_2L_8 unit with a mean torsion angle χ = 3.5 [7]°. The Mo–Mo bond distance of 2.114(2) Å is shorter by ~0.08 Å than that in $[Mo_2(CN)_8]^{4-}$, but slightly longer than the corresponding distance in $Mo_2(O_2CCH_3)_4$. The C≡N bond distances in **2**, none of which are related by crystallographic symmetry, vary from 1.09 to 1.19 Å. These differences are ascribed to packing influences of the anion with the tetrabutylammonium cations, as evidenced by close contacts (2.4–2.8 Å) between two $[Bu^n_4N]^+$ cations and the N atoms of several cyanide ligands. Important bond distances and angles for **2** are provided in Table 9.

*$[Bu^n_4N]_2[Re_2(CN)_6(dppm)_2]\cdot 8CH_2Cl_2$ (**4**·$8CH_2Cl_2$)*

The single crystal X-ray structure of $[Bu^n_4N]_2[Re_2(CN)_6(dppm)_2]\cdot 8CH_2Cl_2$ is quite unusual for several reasons. Firstly, it is the only example of an edge-sharing compound that clearly falls into the category of a $Re_2^{II,II}$ rather than a $Re_2^{III,III}$ species, secondly the anion $[Re_2(CN)_6(dppm)_2]^{2-}$ is the first $[M_2L_{10}]^{2-}$ species to be reported, and thirdly it contains a very rare mode of coordination for the cyanide ligand. The full ORTEP is depicted in Fig. 3, and a skeletal viewpoint of the equatorial plane is provided in Fig. 4. Selected bond distances and angles are provided in Table 10. It can be seen from the drawing in Fig. 4 that the four terminal cyanide and two bridging cyanide ligands are arranged in a pseudo edge-sharing bioctahedral arrangement. The bridging cyanide ions are bound to the Re–Re unit in an η^2 fashion consisting of a σ bond between C(1) and Re(1) and a π interaction between the C(1)≡N(1) moiety and Re(1)*. This type of situation has been crystallographically documented in only one

TABLE 9. Selected bond distances (Å) and bond angles (°) and their e.s.d.s for $[Bu^n_4N]_3[Mo_2(O_2CCH_3)(CN)_6]$ (**2**)

Bond distances			
Mo(1)–Mo(2)	2.114(2)	O(1)–C(7)	1.29(2)
Mo(1)–O(1)	2.13(1)	O(2)–C(7)	1.26(2)
Mo(1)–C(1)	2.16(2)	N(1)–C(1)	1.16(2)
Mo(1)–C(2)	2.23(3)	N(2)–C(2)	1.13(3)
Mo(1)–C(3)	2.21(2)	N(3)–C(3)	1.11(2)
Mo(2)–O(2)	2.13(1)	N(4)–C(4)	1.09(2)
Mo(2)–C(4)	2.22(2)	N(5)–C(5)	1.16(2)
Mo(2)–C(5)	2.17(2)	N(6)–C(6)	1.19(2)
Mo(2)–C(6)	2.14(2)	C(7)–C(8)	1.49(3)
Bond angles			
Mo(2)–Mo(1)–O(1)	91.3(4)	O(2)–Mo(2)–C(6)	84.4(6)
Mo(2)–Mo(1)–C(1)	107.3(5)	C(4)–Mo(2)–C(5)	89.7(7)
Mo(2)–Mo(1)–C(2)	104.5(5)	C(4)–Mo(2)–C(6)	89.8(8)
Mo(2)–Mo(1)–C(3)	101.5(6)	C(5)–Mo(2)–C(6)	143.7(7)
O(1)–Mo(1)–C(1)	161.4(6)	Mo(1)–O(1)–C(7)	118(1)
O(1)–Mo(1)–C(2)	91.9(7)	Mo(2)–O(2)–C(7)	119(1)
O(1)–Mo(1)–C(3)	89.8(6)	Mo(1)–C(1)–N(1)	169(2)
C(1)–Mo(1)–C(2)	84.6(7)	Mo(1)–C(2)–N(2)	170(2)
C(1)–Mo(1)–C(3)	85.5(6)	Mo(1)–C(3)–N(3)	174(2)
C(2)–Mo(1)–C(3)	153.9(7)	Mo(2)–C(4)–N(4)	179(2)
Mo(1)–Mo(2)–O(2)	91.1(4)	Mo(2)–C(5)–N(5)	170(1)
Mo(1)–Mo(2)–C(4)	104.5(6)	Mo(2)–C(6)–N(6)	169(2)
Mo(1)–Mo(2)–C(5)	108.7(5)	O(1)–C(7)–O(2)	119(2)
Mo(1)–Mo(2)–C(6)	106.5(6)	O(1)–C(7)–C(8)	117(2)
O(2)–Mo(2)–C(4)	164.4(7)	O(2)–C(7)–C(8)	123(2)
O(2)–Mo(2)–C(5)	86.4(5)		

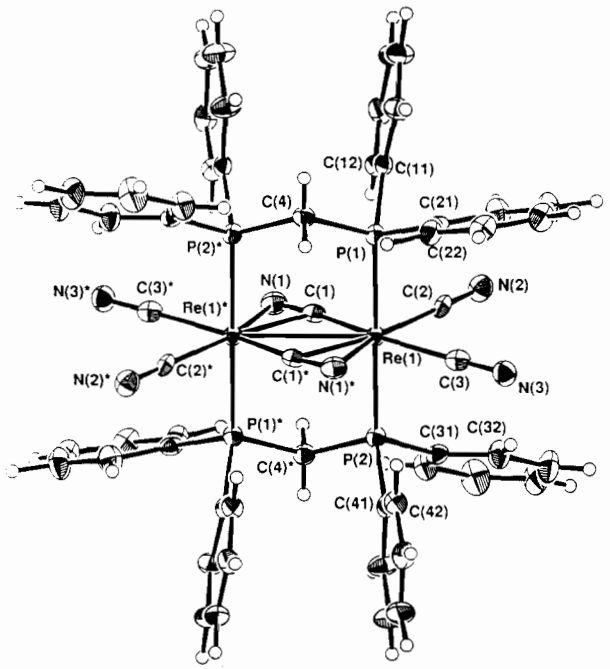

Fig. 3. ORTEP plot of a molecule of $[Re_2(CN)_6(dppm)_2]^{2-}$ with non-hydrogen atoms represented by their 50% probability ellipsoids.

previous instance, namely in the dimolybdenum complex $[Bu^n_4N][Cp_2Mo_2(CO)_4(CN)]$ [30a]. This unsymmetrical bridging CN mode has been documented in two other

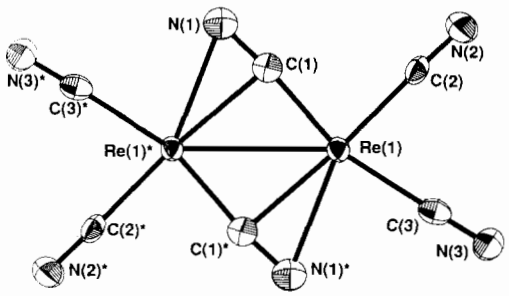

Fig. 4. View looking down on the equatorial plane of the anion $[Re_2(CN)_6(dppm)_2]^{2-}$ emphasizing the unsymmetrical arrangement of the bridging CN group.

TABLE 10. Selected bond distances (Å) and bond angles (°) and their e.s.d.s for $[Bu^n_4N]_2[Re_2(CN)_6(dppm)_2]\cdot 8CH_2Cl_2$ (**4**·$8CH_2Cl_2$)

Bond distances			
Re(1)*–Re(1)	3.0505(6)	P(1)–C(11)	1.834(6)
Re(1)–P(1)	2.369(2)	P(1)–C(21)	1.819(7)
Re(1)–P(2)	2.379(2)	P(2)–C(4)*	1.838(7)
Re(1)–N(1)*	2.486(6)	P(2)–C(31)	1.834(6)
Re(1)–C(1)	2.002(7)	P(2)–C(41)	1.830(7)
Re(1)–C(1)*	2.311(6)	N(1)–C(1)	1.177(8)
Re(1)–C(2)	2.070(7)	N(2)–C(2)	1.155(8)
Re(1)–C(3)	2.105(7)	N(3)–C(3)	1.161(8)
P(1)–C(4)	1.836(7)		
Bond angles			
Re(1)*–Re(1)–P(1)	89.90(4)	C(2)–Re(1)–C(3)	79.3(2)
Re(1)*–Re(1)–P(2)	90.08(4)	Re(1)–P(1)–C(4)	113.6(2)
Re(1)*–Re(1)–C(1)	49.3(2)	Re(1)–P(1)–C(11)	122.6(2)
Re(1)*–Re(1)–C(1)*	41.0(2)	Re(1)–P(1)–C(21)	112.5(2)
Re(1)*–Re(1)–C(2)	133.8(2)	C(4)–P(1)–C(11)	101.3(3)
Re(1)*–Re(1)–C(3)	146.9(2)	C(4)–P(1)–C(21)	103.4(3)
P(1)–Re(1)–P(2)	179.56(6)	C(11)–P(1)–C(21)	101.1(3)
P(1)–Re(1)–C(1)	93.5(2)	Re(1)–P(2)–C(4)*	112.9(2)
P(1)–Re(1)–C(1)*	86.9(2)	Re(1)–P(2)–C(31)	116.2(2)
P(1)–Re(1)–C(2)	88.5(2)	Re(1)–P(2)–C(41)	120.2(2)
P(1)–Re(1)–C(3)	91.9(2)	C(4)*–P(2)–C(31)	102.0(3)
P(2)–Re(1)–C(1)	86.8(2)	C(4)*–P(2)–C(41)	103.6(3)
P(2)–Re(1)–C(1)*	92.8(2)	C(31)–P(2)–C(41)	99.2(3)
P(2)–Re(1)–C(2)	91.9(2)	Re(1)–C(1)–Re(1)*	89.7(2)
P(2)–Re(1)–C(3)	87.9(2)	Re(1)–C(1)–N(1)	173.4(6)
C(1)–Re(1)–C(1)*	90.3(2)	Re(1)–C(1)*–N(1)*	84.2(4)
C(1)–Re(1)–C(2)	84.8(2)	Re(1)–C(2)–N(2)	178.1(6)
C(1)–Re(1)–C(3)	163.0(2)	Re(1)–C(3)–N(3)	178.2(6)
C(1)*–Re(1)–C(2)	173.0(2)	P(1)–C(4)–P(2)*	112.3(3)
C(1)*–Re(1)–C(3)	106.1(2)		

cases, $[Mn_2H(CN)(CO)_4(dppm)_2]$ and $[Rh_2(CN)(CO)_3(dppm)_2]ClO_4$, but full structural details were not available [30b, c]. In the Mo structure, however, a disorder associated with the bridging cyanide precluded the reliable determination of bond distances and angles associated with this unusual mode of CN^- binding. The bridging angle ⟨Re(1)–C(1)–N(1) is 173.4(6)° in $[Re_2(CN)_6(dppm)_2]^{2-}$ compared to the angle ⟨Mo–C–N_{bridge} = 170° in $[Cp_2Mo_2(CO)_4(CN)]^-$. Other salient features in **4** are Re(1)–C(1) = 2.002(7),

Re(1)*–C(1) = 2.311(6), Re(1)*–N(1) = 2.486(6) and C(1)–N(1) = 2.177(8) Å. It is interesting to note that the unstable phosphorous analog of the $C{\equiv}N^-$ ligand, $C{\equiv}P^-$, has recently been documented as a bridging moiety in the complex $(Cl)(PEt_3)_2Pt(\mu\text{-}C{\equiv}P)Pt(PEt_3)_2$ [31]. There are major differences in the present example and the Pt case, however, as the $C{\equiv}P^-$ ligand does not span an M–M bonding interaction and the Pt–C–P angle (144.0°) is bent, unlike the Re–C–N angle (173.4°). The Re–Re distance in $[Re_2(CN)_6(dppm)_2]^{2-}$ of 3.0505(6) Å is in accord with an Re–Re single bond ($\sigma^2\pi^2(\delta^2\delta^{*2})\pi^{*2}$); magnetic and NMR data are in perfect agreement with this assignment (*vide supra*).

$[Re_2(MeCN)_{10}][Mo_6O_{19}]_2$ (6)

Selected metric parameters are presented in Table 11. The structure of **6** consists of discrete cation and anion units in the expected 1:2 ratio. The salt crystallizes in the space group *C2/c* with the midpoint of the Re–Re bond residing on a two-fold symmetry axis. As can be seen in Fig. 5, the environment of the Re(II) centers is pseudo-octahedral, consisting of four, nearly planar CH_3CN moieties with the two additional vertices defined by a weakly interacting axial CH_3CN group and the other Re atom. In contrast to the corresponding cation $[Mo_2(MeCN)_{10}]^{4+}$ which exhibits an eclipsed M_2L_8 geometry [8], the dirhenium unit is perfectly staggered with a mean torsion angle $\chi = 44.5[1]°$. The Re–Re distance of 2.259(4) Å is comparable to the M–M distances in dirhenium complexes containing M–M triple bonds of the electron-rich $\sigma^2\pi^4\delta^2\delta^{*2}$ configuration. A three-dimensional packing diagram within a 10 Å radius from the center of the Re–Re bond revealed that the cation resides in pseudo-octahedral sites formed by the $[Mo_6O_{19}]^{2-}$ anions, suggesting a fluorite structure.

TABLE 11. Selected bond distances (Å) and bond angles (°) and their e.s.d.s for $[Re_2(MeCN)_{10}][Mo_6O_{19}]_2 \cdot 4CH_3CN \cdot 2H_2O$ ($\mathbf{6} \cdot 4CH_3CN \cdot 2H_2O$)

Bond distances			
Re1–Re1*	2.259(4)	N3–C5	1.18(3)
Re1–N1	2.07(3)	N4–C7	1.13(4)
Re1–N2	2.02(2)	N5–C9	1.09(3)
Re1–N3	2.06(2)	C1–C2	1.33(5)
Re1–N4	2.16(3)	C3–C4	1.47(4)
Re1–N5	2.51(3)	C5–C6	1.37(4)
N1–C1	1.06(3)	C9–C10	1.39(4)
N2–C3	1.12(3)		
Bond angles			
Re1–Re1*–N2	92.6(7)	N2–C3–C4	172(3)
Re1–Re1*–N5	174.6(6)	Re1–N5–C9	168(3)
Re1–N1–C1	170(3)	N5–C9–C10	178(4)
N1–C1–C2	179(4)		

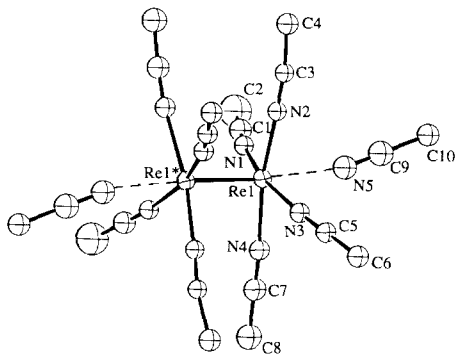

Fig. 5. ORTEP representation of the cation in the salt $[Re_2(MeCN)_{10}][Mo_6O_{19}]_2$ at the 40% probability ellipsoids.

$[Rh_2(MeCN)_{10}][Mo_6O_{19}]_2$ (7·4CH₃CN)

Important structural features of this salt are compiled in Table 12. Figure 6 depicts an ORTEP plot of the molecular cation and the two $[Mo_6O_{19}]^{2-}$ anions. In addition to these moieties, the salt contains four molecules of CH_3CN in the lattice. This compound is the second example of a crystallographically characterized salt containing the dirhodium solvated cation $[Rh_2(MeCN)_{10}]^{4+}$, the other being the $[BF_4]^-$ salt [3]. There are no remarkable differences in the two cations except for minor changes in metric parameters that reflect packing influences. The Rh–Rh interaction in **7** is 2.616(3) and 2.624(1) Å in the $[BF_4]^-$ structure. As in the previous case, the cation adopts an essentially staggered arrangement of $Rh(MeCN)_4$ units ($\chi_{av} = 45.0[8]$).

New oxide materials from acetonitrile cation salts of $[Mo_6O_{19}]^{2-}$

Besides affording ease of crystallization, the polyoxometallate salts in this study allow for the mild synthesis of new solid-state compounds. The Mo, Re and Rh solvated compounds of $[Mo_6O_{19}]^{2-}$ reveal quantitative loss of acetonitrile ligands upon prolonged heating up

TABLE 12. Selected bond distances (Å) and bond angles (°) and their e.s.d.s for $[Rh_2(MeCN)_{10}][Mo_6O_{19}]_2 \cdot 4CH_3CN$ ($\mathbf{7} \cdot 4CH_3CN$)

Bond distances			
Rh1–Rh1*	2.616(3)	N3–C4	1.18(3)
Rh1–N1	1.97(2)	N4–C5	1.13(2)
Rh1–N2	1.97(2)	N5–C1	1.14(2)
Rh1–N3	2.14(2)	C1–C10	1.52(3)
Rh1–N4	1.98(2)	C2–C6	1.54(3)
Rh1–N5	1.97(2)	C3–C7	1.51(3)
N1–C2	1.12(2)	C4–C8	1.54(3)
N2–C3	1.14(3)		
Bond angles			
Rh1–Rh1*–N1	92.2(5)	Rh1–N2–C3	175(2)
Rh1–Rh1*–N2	88.2(5)	N2–C3–C7	178(2)
Rh1–Rh1*–N3	177.6(5)	Rh1–N3–C4	168(2)
Rh1–N1–C2	167(2)	N3–C4–C8	179(2)
N1–C2–C6	175(3)		

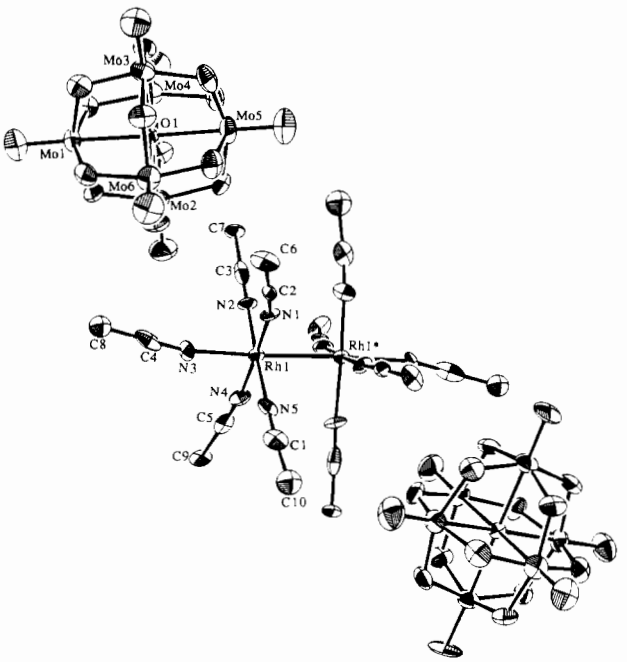

Fig. 6. Molecular structures of the constituent ions in $[Rh_2(MeCN)_{10}][Mo_6O_{19}]_2$ with atoms represented by their 40% probability ellipsoids.

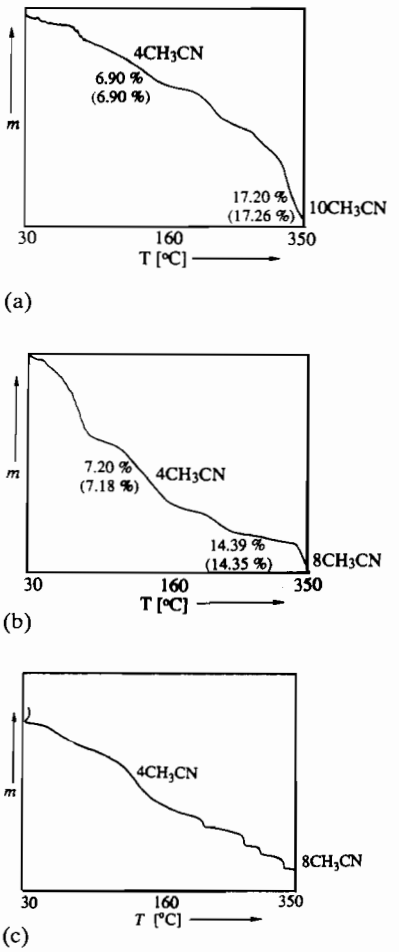

Fig. 7. Thermogravimetric analyses measurements for: (a) $[Rh_2(MeCN)_{10}][Mo_6O_{19}]_2$, (b) $[Mo_2(MeCN)_{10}][Mo_6O_{19}]_2$, (c) $[Re_2(MeCN)_{10}][Mo_6O_{19}]_2$. Experimental weight losses are given directly beneath the curve and the theoretical weight losses are listed in parentheses.

to 350 °C. The TGA curves for compounds **6**, **7** and **10**, depicted in Fig. 7, show major plateaus corresponding to loss of four, six and eight acetonitrile ligands. The IR spectra of the resulting black solids $M'Mo_6O_{19}$ ($M' = Rh$ (**13**); Mo (**14**); Re (**15**)) are essentially featureless except for strong absorptions in the range of M–O stretches (400–1000 cm^{-1}). Identical materials were obtained in bulk by heating samples of **6**, **7** and **10** under similar conditions in a temperature programmed tube furnace. Attempts to characterize the oxides included powder X-ray diffraction and X-ray photoelectron spectroscopy (XPS). Preliminary XPS studies of **13–15** indicate that the materials are free of carbon or nitrogen impurities and that the surface ratio of metal atoms is approximately 0.1 for Rh:Mo in '$RhMo_6O_{19}$' and Re:Mo in '$ReMo_6O_{19}$'. All samples exhibited Mo 3d binding energies typical for Mo^{6+}; the Re 4f binding energies for **13** indicated multiple oxidation states of Re (3^+, 4^+, 5^+). The Rh 3d binding energies for **15** point to a single oxidation state, most likely Rh^{3+}. These samples are currently being studied under anaerobic conditions to avoid contamination from possible oxidation products at the surface. To our knowledge, there is only one documented example of a ternary Rh/Mo oxide [32] and no reported instances of a Re/Mo oxide. Investigations are underway to characterize these materials by small angle neutron scattering studies which will help to establish bulk purity and composition, and EXAFS which will provide valuable structural information regarding the fate of the dimetal unit in the desolvated oxide materials. The Re/Mo and Rh/Mo oxides are amorphous, but the purely Mo oxide **14** derived from $[Mo_2(MeCN)_{10}][Mo_6O_{19}]_2$ is highly crystalline with tetragonal cell parameters $a = b = 10.811$, $c = 2.819$ Å, $V = 329.5$ Å^3. The powder pattern is displayed in Fig. 8. According to a search of powder X-ray databases, this particular Mo/oxide has not been reported.

Conclusions and future outlook

Besides being fascinating molecules in their own right, the compounds reported in this study show promise for the synthesis of new materials incorporating metal–metal bonded dinuclear complexes. The properties of the acetonitrile cations and their chemistry with polyoxometallates are of considerable interest in the context of the mild synthesis of new mixed-metal

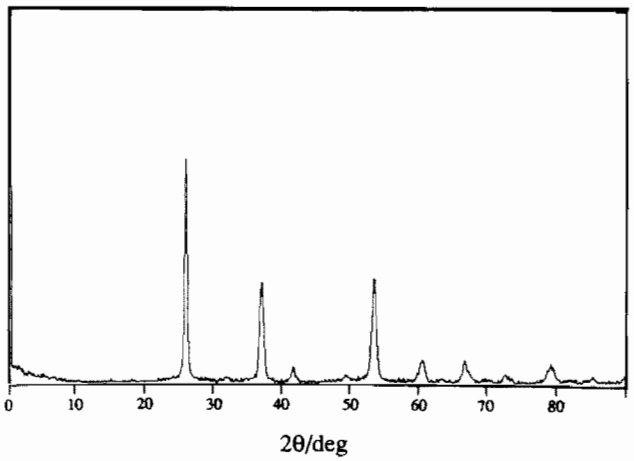

Fig. 8. Powder X-ray pattern for the material **14** resulting from thermal treatment of $[Mo_2(MeCN)_{10}][Mo_6O_{19}]_2$.

oxides by molecular approaches. The isolation of the crystalline phase prepared from thermal treatment of $[Mo_2(MeCN)_{10}][Mo_6O_{19}]_2$ supports the feasibility of unearthing new solid-state compounds that are not accessible by conventional high temperature routes. Furthermore, the solids prepared from desolvation of the cation in oxide-containing salts may find valuable applications in heterogeneous catalysis. An advantage of the present method is that lower temperatures provide materials wherein the stoichiometry of the constituent metal atoms is exact and the metal atoms are evenly mixed within the precursor salts. Future directions for the homoleptic cyanide compounds in materials include their reactions with cations to form mixed-metal compounds wherein the cyanide ligand behaves as a linear bridging group. From a purely structural point of view, the eight-coordinate anion $[Mo_2(CN)_8]^{4-}$ would be expected to be a good match for tetrahedral cations. In light of the recent flurry of activity regarding 'supramolecular architecture' [21e] and ferromagnetism [33] of cyanide materials, it is an intriguing and timely idea to make use of metal–metal bonded building blocks with different shapes and sizes as well as rich redox properties.

Acknowledgements

We gratefully acknowledge the National Science Foundation (Grant CHE-89149), the Center for Fundamental Materials Research at Michigan State University, the Camille and Henry Dreyfus Foundation and the Alfred P. Sloan Foundation for providing funding. (K.R. Dunbar is a Camille and Henry Dreyfus Teacher and Scholar Fellow of the Alfred P. Sloan Foundation.) We thank Dr J. Amarasekera and Professor T.J. Pinnavaia for help with the TGA analyses, Professor J. Ledford for the XPS studies and Dr D. Ward for help with X-ray crystallography. The single crystal X-ray equipment was supported by the National Science Foundation (CHE-8403823 and CHE-8908088). The powder X-ray diffractometer was supported by the Center for Fundamental Materials Research at Michigan State University. NMR equipment was provided by the National Science Foundation (Grant CHE-88-00770) and the National Institutes of Health (Grant No. 1-S10-RR04750-01).

References

1 (a) F.A. Cotton, N.F. Curtis, C.B. Harris, B.F.G. Johnson, S.J. Lippard, J.T. Mague, W.R. Robinson nd J.S. Wood, *Science, 145* (1964) 1305; (b) F.A. Cotton and R.A. Walton, *Multiple Bonds Between Metal Atoms,* Oxford University Press, Oxford, 2nd. edn., 1993.
2 (a) R.H. Cayton and M.H. Chisholm, *J. Am. Chem. Soc., 111* (1989) 8921; (b) R.H. Cayton, M.H. Chisholm and F.D. Darrington, *Angew. Chem., Int. Ed. Engl., 29* (1990) 1481; (c) M.H. Chisholm, *Angew. Chem., Int. Ed. Engl., 30* (1991) 673.
3 K.R. Dunbar, *J. Am. Chem. Soc., 110* (1988) 8247.
4 S.N. Bernstein and K.R. Dunbar, *Angew. Chem., Int. Ed. Engl., 31* (1992) 1359.
5 A.B. Brignole and F.A. Cotton, *Inorg. Synth., 13* (1972) 81.
6 F.A. Cotton and J.G. Norman, *Coord. Chem., 1* (1971) 14.
7 K.R. Dunbar and L.E. Pence, *Inorg. Synth., 29* (1992) 182.
8 F.A. Cotton and K.J. Wiesinger, *Inorg. Chem., 30* (1991) 871.
9 T.J. Barder, F.A. Cotton, K.R. Dunbar, G.L. Powell, W. Schwotzer and R.A. Walton, *Inorg. Chem., 24* (1985) 2550.
10 (a) T.J. Barder and R.A. Walton, *Inorg. Chem., 21* (1982) 2510; (b) *Inorg. Synth., 23* (1985) 116.
11 J.R. Ebner and R.A. Walton, *Inorg. Chem., 14* (1975) 1987.
12 M. Che, M. Fournier and J.P. Launay, *J. Chem. Phys., 71* (1979) 1954.
13 W.G. Klemperer, *Inorg. Synth., 27* (1990) 713.
14 S. Andreades and E.W. Zahnow, *J. Am. Chem. Soc., 91* (1969) 4181.
15 (a) A. Bino, F.A. Cotton and P.E. Fanwick, *Inorg. Chem., 18* (1979) 3558; (b) F.A. Cotton, B.A. Frenz, G. Deganello and A. Shaver, *J. Organomet. Chem.,* (1973) 227.
16 *TEXSAN-TEXRAY Structure Analysis Package,* Molecular Structure Corporation, The Woodlands, TX, 1985.
17 C.J. Gilmore, *J. Appl. Crystallogr., 17* (1984) 42.
18 R.T. Beurskens, DIRDIF: Direct Methods for Difference Structure, an automatic procedure for phase extension; refinement of difference structure factors, *Tech. Rep. 1984/1,* Crystallography Laboratory, Toernooivelt, 6525 Ed Nijmegen, Netherlands, 1984.
19 N. Walker and D. Stuart, *Acta Crystallogr., Sect. A, 39* (1983) 158–166.
20 G.M. Sheldrick, in G.M. Sheldrick, C. Kruger and R. Goddard (eds.), *Crystallographic Computing 3,* Oxford University Press, Oxford, 1985, pp. 175–189.
21 (a) A.G. Sharpe, *The Chemistry of Cyano Complexes of the Transition Metals,* Academic Press, London, 1976; (b) A. Ludi, H.U. Güdel, *Struct. Bonding (Berlin), 14* (1973) 1–21; (c) D.F. Shriver, *Struct. Bonding (Berlin), 1* (1966) 32–58; (d) W.P. Griffith, *Coord. Chem. Rev., 17* (1975) 177–247; (e) T. Iwamoto, in J.L. Atwood, J.E.D. Davies and D.D. MacNicol (eds.), *Inclusion Compounds: Inorganic and Physical Aspects of Inclusion,* Vol. 5, Oxford University Press, Oxford, 1991, Ch. 6, pp. 177–212.
22 C.D. Garner and R.G. Senior, *J. Chem. Soc., Dalton Trans.,* (1975) 1171.

23 P.E. Fanwick, D.S. Martin, F.A. Cotton and T.R. Webb, *Inorg. Chem., 16* (1977) 2103.

24 L.B. Anderson, T.J. Barder, F.A. Cotton, K.R. Dunbar, L.R. Falvello and R.A. Walton, *Inorg. Chem., 25* (1986) 3629.

25 T.J. Barder, F.A. Cotton, D. Lewis, W. Schwotzer, S.M. Tetrick and R.A. Walton, *J. Am. Chem. Soc., 106* (1984) 2882.

26 (a) C. Rocchiccioli-Deltcheff, R. Thouvenot and M. Fouassier, *Inorg. Chem., 21* (1982) 30; (b) C. Rocchiccioli-Deltcheff, R. Fournier and R. Thouvenot, *Inorg. Chem., 22* (1983) 207; (c) C. Rocchiccioli-Deltcheff, M. Fournier, R. Frank and R. Thouvenot, *Spectrosc. Lett., 19* (1986) 765.

27 J.V. Brencic and F.A. Cotton, *Inorg. Chem., 8* (1969) 7.

28 F.A. Cotton, Z.C. Mester and T. Webb, *Acta Crystallogr., Sect. B, 30* (1974) 2768.

29 (a) P.A. Bates, A.J. Nielson and J.M. Waters, *Polyhedron, 6* (1987) 2111; (b) K.R. Breakell, S.J. Rettig, A. Storr and J. Trotter, *Can. J. Chem., 61* (1983) 1659; (c) F.A. Cotton, W.J. Ilsley and W. Kaim, *Inorg. Chem., 20* (1981) 930; (d) F.A. Cotton and W.H. Ilsley, *Inorg. Chem., 20* (1981) 572.

30 (a) D.M. Curtis, K.R. Han and W.M. Butler, *Inorg. Chem., 16* (1980) 2096; (b) H.C. Aspinall, A.J. Deeming and S. Donovan-Mtunzi, *J. Chem. Soc., Dalton Trans.,* (1983) 2669; (c) S.P. Deraniyagala and K.R. Grundy, *Inorg. Chim. Acta, 84* (1984) 205.

31 H. Jun, V.G. Young, Jr. and R.J. Angelici, *J. Am. Chem. Soc., 114* (1992) 10064.

32 J. Badaud, *C. R. Seances Acad. Sci. Ser. C, 284* (1977) 921.

33 V. Gadet, T. Mallah, I. Castro and M. Verdaguer, *J. Am. Chem. Soc., 114* (1992) 9213.